Cell Reports

Article

Specific connectivity optimizes learning in thalamocortical loops

Graphical abstract

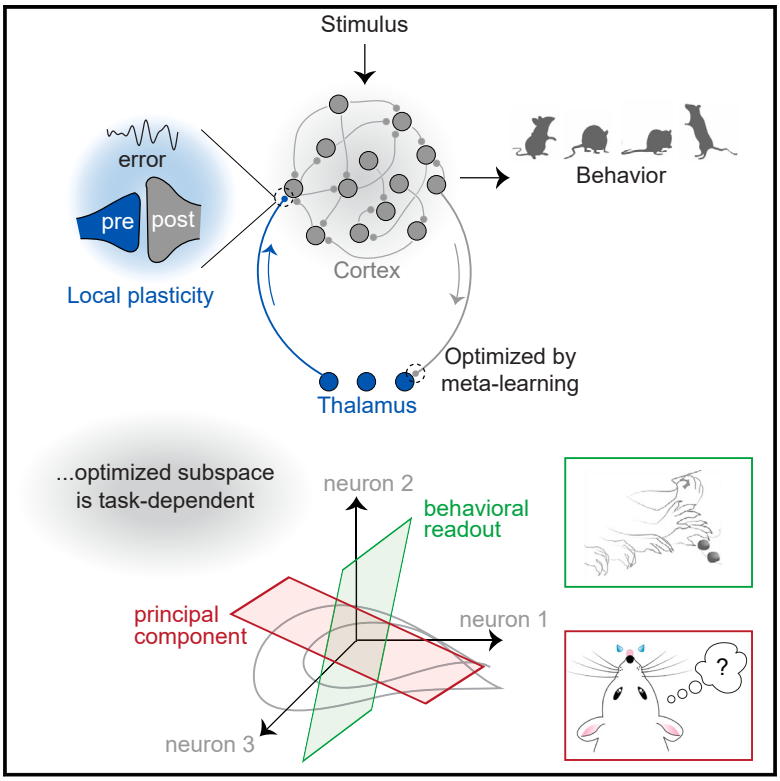

Highlights

- Learning via thalamocortical plasticity depends on corticothalamic connectivity
- Meta-learning identifies optimal corticothalamic connectivity for learning different tasks
- Readout/principal-component-aligned connectivity optimizes motor control/working memory
- Neural recordings from the mouse cortex and thalamus validate the model

Authors

Kaushik J. Lakshminarasimhan, Marjorie Xie, Jeremy D. Cohen, Britton A. Sauerbrei, Adam W. Hantman, Ashok Litwin-Kumar, Sean Escola

Correspondence

a.litwin-kumar@columbia.edu (A.L.-K.), sean@neurotheory.columbia.edu (S.E.)

In brief

A growing body of evidence shows that higher-order thalamus shapes cortical dynamics. Lakshminarasimhan et al. investigate a computational model of thalamocortical loops and show that task-specific structured corticothalamic connectivity is needed for learning via thalamocortical synapses. The authors validate their predictions using neural recordings from mice.

Lakshminarasimhan et al., 2024, Cell Reports *43*, 114059
April 23, 2024
https://doi.org/10.1016/j.celrep.2024.114059

CellPress

Cell Reports

CellPress
OPEN ACCESS

Article

Specific connectivity optimizes learning in thalamocortical loops

Kaushik J. Lakshminarasimhan,[1] Marjorie Xie,[1] Jeremy D. Cohen,[2] Britton A. Sauerbrei,[3] Adam W. Hantman,[2] Ashok Litwin-Kumar,[1,*] and Sean Escola[4,5,*]

[1]Zuckerman Mind Brain Behavior Institute, Columbia University, New York, NY 10027, USA
[2]Neuroscience Center, University of North Carolina, Chapel Hill, NC 27559, USA
[3]Department of Neurosciences, Case Western Reserve University, Cleveland, OH 44106, USA
[4]Department of Psychiatry, Columbia University, New York, NY 10032, USA
[5]Lead contact
*Correspondence: a.litwin-kumar@columbia.edu (A.L.-K.), sean@neurotheory.columbia.edu (S.E.)
https://doi.org/10.1016/j.celrep.2024.114059

SUMMARY

Thalamocortical loops have a central role in cognition and motor control, but precisely how they contribute to these processes is unclear. Recent studies showing evidence of plasticity in thalamocortical synapses indicate a role for the thalamus in shaping cortical dynamics through learning. Since signals undergo a compression from the cortex to the thalamus, we hypothesized that the computational role of the thalamus depends critically on the structure of corticothalamic connectivity. To test this, we identified the optimal corticothalamic structure that promotes biologically plausible learning in thalamocortical synapses. We found that corticothalamic projections specialized to communicate an efference copy of the cortical output benefit motor control, while communicating the modes of highest variance is optimal for working memory tasks. We analyzed neural recordings from mice performing grasping and delayed discrimination tasks and found corticothalamic communication consistent with these predictions. These results suggest that the thalamus orchestrates cortical dynamics in a functionally precise manner through structured connectivity.

INTRODUCTION

Recent years have seen a renewal of interest in understanding the role of the higher-order thalamus in mammalian behavior. Unlike primary thalamic nuclei, such as the lateral geniculate nucleus, which relays information from the sensory periphery to the cortex, higher-order nuclei do not receive direct inputs from the sensory periphery but rather primarily from layer V neurons in the cortex. Consequently, the conventional view of the thalamus as a relay has been revised to accommodate a role for the higher-order thalamus as a "higher-order relay" that transmits information from one cortical area to another.[1,2] Meanwhile, anatomical tracing studies have revealed a frequent motif of reciprocal interactions in which cortical projections to the thalamus target nuclei that project back to the same cortical area. Such reciprocal cortico-thalamo-cortical (CTC) loops have been observed in rodent sensory,[3] motor,[4–7] and prefrontal[8] cortices and stand in contrast to a view of such nuclei as higher-order relays across cortical areas. Recent physiological studies have demonstrated that these loops are required for many cognitive functions.[9–13] Furthermore, the evolution of cortical activity depends on the thalamus[14] and inhibiting the higher-order thalamus suppresses cortical activity.[10,11] However, the specific computational role of CTC loops is not fully understood.

Reciprocal CTC loops represent a departure from the labeled line view of the thalamus as they feature signal compression (from the cortex to the thalamus) and expansion (from the thalamus to the cortex). Normative models developed to clarify the role of compression and expansion in feedforward neural networks have improved our understanding of the computations in many brain areas including the retina,[15,16] primary visual cortex,[17,18] olfactory bulb,[19,20] and cerebellum.[21–24] For instance, theories of compressed sensing and efficient coding have shown that, whereas random compression can preserve the similarity structure of sparse representations, the optimal compression strategy is to extract the principal components (PCs) when inputs are strongly correlated.[25] Unfortunately, insights gained from analyzing feedforward networks cannot be directly applied to understand signal transformation in CTC loops due to their recurrent processing.

We and others have shown in prior theoretical studies that it is possible to perform computations by tuning synaptic weights in the CTC loop appropriately,[26–28] consistent with experimental studies showing that thalamocortical synapses exhibit plasticity in many areas of the adult brain.[29–35] Such plasticity can be viewed as low-rank modifications to the connectivity of cortical recurrent neural networks.[36–38] However, these models have not addressed how these synapses may be updated with biologically plausible learning rules that operate using locally available signals. In particular, we show that standard approaches for local, biologically plausible learning in

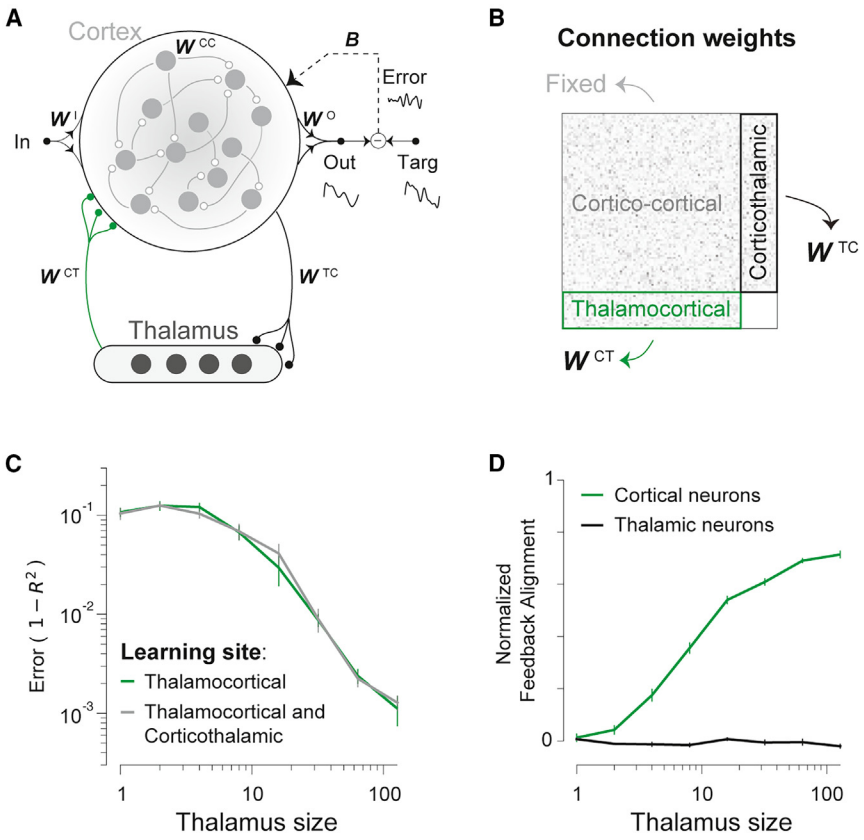

Figure 1. Combined model of cortex and thalamus

(A) Schematic illustration of a thalamocortical network model.

(B) Synaptic weights of the model. Corticocortical weights ($\boldsymbol{W}^{CC}$) are fixed. Local learning rules can be used to update thalamocortical weights ($\boldsymbol{W}^{CT}$), but it is not known whether such rules are effective for corticothalamic weights ($\boldsymbol{W}^{TC}$).

(C) Learning performance (quantified as $1 - R^2$, so lower is better) as a function of thalamic population size when learning is mediated by a local plasticity rule (RFLO) in thalamocortical weights (green), or both thalamocortical and corticothalamic weights (gray).

(D) The alignment between feedback weights ($\boldsymbol{B}$) and readout weights ($\boldsymbol{W}^{O}$) in cortical neurons increases as learning performance improves, indicating successful credit assignment in thalamocortical synapses (green). In contrast, there is no alignment between feedback weights ($\boldsymbol{B}'$, see Figure S1A) and effective readout weights ($\boldsymbol{W}^{CT}\varphi'(\mathbf{u}_t)\boldsymbol{W}^{O}$, where $\mathbf{u}_t$ denotes the membrane potential of cortical neurons, see STAR Methods) in thalamic neurons indicating the failure of credit assignment in corticothalamic synapses (black). Numerical estimates of alignment (β) are normalized to correct for the chance level alignment (β_0) before plotting $(\beta - \beta_0)/(1 - \beta_0)$. Models have $N = 256$ cortical neurons. The number of thalamic neurons (M) is varied from 1 to 128. Error bars denote standard errors estimated by bootstrapping. See also Figure S1.

recurrent neural networks fail to optimize corticothalamic connectivity, because accurate credit assignment at these synapses requires knowledge of the global structure of network activity.

In this study, we hypothesize that the ability of the thalamus to contribute to learning depends critically on the structure of corticothalamic synaptic connectivity and ask what forms of corticothalamic connectivity structure optimize learning. We use a recently proposed biologically plausible, three-factor supervised learning rule[39] to update thalamocortical synapses, while assuming that corticothalamic synapses have been optimized on a slower evolutionary or developmental timescale.[40,41] We separately train models to perform two different tasks—autonomous motor control and working memory—and determine the optimal corticothalamic structure in each case. We find that the optimal corticothalamic connectivity is structured and task dependent. Specifically, learning motor control is optimized by corticothalamic connections specialized to carry an efferent copy of the muscle command, while learning to perform working memory is optimized by corticothalamic connections that convey modes of cortical activity with the highest variance. We analyzed neural recordings from mice performing grasping and delayed discrimination tasks[10,14] and found that the influence of cortical activity on the thalamus is consistent with this model. These results suggest a precise link between corticothalamic connectivity structure and the function of CTC loops.

RESULTS

We begin by constructing a model combining cortex and thalamus based on two fundamental properties of thalamic nuclei that distinguish them from the cortex. First, there are far fewer neurons in the thalamus,[42] which acts as a structural bottleneck in this loop. Second, local recurrent excitation is a defining feature of the cortex but absent within the thalamus.[43,44] Therefore, we consider a model in which a network of N interconnected cortical neurons is reciprocally connected with M uncoupled thalamic neurons, with $M \ll N$ (Figure 1A). The cortical population activity is denoted by $\mathbf{h}_t \in \mathbb{R}^N$, thalamic population activity by $\mathbf{r}_t \in \mathbb{R}^M$, and S external inputs (if any) by $\mathbf{x}_t \in \mathbb{R}^S$. The cortical activity evolves according to:

$$\tau\dot{\mathbf{h}}_t = -\mathbf{h}_t + \varphi\left(\boldsymbol{W}^{CC}\mathbf{h}_t + \boldsymbol{W}^{CT}\mathbf{r}_t + \boldsymbol{W}^{I}\mathbf{x}_t\right), \qquad \text{(Equation 1)}$$

where subscripts denote time, τ is the neuronal time constant, and the nonlinearity $\varphi(\cdot)$ is the tanh function. $\boldsymbol{W}^{CC} \in \mathbb{R}^{N\times N}$, $\boldsymbol{W}^{CT} \in \mathbb{R}^{N\times M}$, and $\boldsymbol{W}^{I} \in \mathbb{R}^{N\times S}$ denote corticocortical, thalamocortical and input weight matrices, respectively. Thalamic activity, on the other hand, is assumed to depend only on cortical activity as $\mathbf{r}_t = \varphi(\boldsymbol{W}^{TC}\mathbf{h}_t)$, where $\boldsymbol{W}^{TC} \in \mathbb{R}^{M\times N}$ denotes the matrix of corticothalamic weights. Therefore, the thalamic activity is a nonlinear M-dimensional projection of the cortical activity. Network output $\mathbf{y}_t \in \mathbb{R}^R$, which we optimize to perform

behavioral tasks, is modeled as a linear readout of the cortical activity, $\mathbf{y}_t = \boldsymbol{W}^{\mathrm{O}}\mathbf{h}_t$ with readout weights $\boldsymbol{W}^{\mathrm{O}} \in \mathbb{R}^{R\times N}$.

In this model, cortical neurons interact directly via corticocortical connections and indirectly via the thalamic bottleneck, which compresses the cortical signal into an M-dimensional space (through $\boldsymbol{W}^{\mathrm{TC}}$) before expanding it back into an N-dimensional space (through $\boldsymbol{W}^{\mathrm{CT}}$). The effective interaction weights (obtained using Euler's method) can be expressed as a sum of recurrent connectivity within the cortex and weights in the CTC loop, $\boldsymbol{W}_{\mathrm{eff}} = \boldsymbol{W}^{\mathrm{CC}} + \boldsymbol{W}^{\mathrm{CT}}\boldsymbol{V}\boldsymbol{W}^{\mathrm{TC}}$, where $\boldsymbol{V} = \mathrm{diag}(\varphi'(\mathbf{v}_t))$ is an $M\times M$ diagonal matrix composed of the derivative of the activity of thalamic neurons. This effective interaction matrix can be viewed as a low-rank (rank-M) perturbation of the $N\times N$ cortical connectivity matrix $\boldsymbol{W}^{\mathrm{CC}}$. Such models are interesting from a computational perspective because recent theoretical work has shown that many tasks can be solved by combining a full-rank random component with appropriate low-rank connectivity structures[36] and that gradient-based learning typically induces low-rank changes in recurrent weights.[37] We ask whether low-rank CTC connectivity can be learned to support behavioral tasks in a biologically plausible manner within our model. Throughout the paper, we describe the key details needed to understand the results of each simulation. Further details can be found in Table S1.

Thalamocortical learning rule

Recent experimental evidence suggests that thalamocortical plasticity continues into adulthood and is a major substrate for learning,[30–35] and inhibiting the thalamus impairs learning.[45] Accordingly, we assume that thalamocortical synapses ($\boldsymbol{W}^{\mathrm{CT}}$, Figure 1B, green) are adjusted such that the overall model minimizes $\sum_t \|\boldsymbol{\varepsilon}_t\|^2$, where $\boldsymbol{\varepsilon}_t = \mathbf{y}_t^* - \mathbf{y}_t$ denotes the mismatch between the network output $\mathbf{y}_t$ and some desired target output function $\mathbf{y}_t^*$. Specifically, we train thalamocortical synapses in the model using a local, biologically plausible learning rule based on a recently proposed algorithm (Random-Feedback-Local-Online, or RFLO, learning; see STAR Methods).[39] The resulting update rule is given by:

$$\delta \boldsymbol{W}_{ij}^{\mathrm{CT}} \propto [\boldsymbol{B}\boldsymbol{\varepsilon}_t]_i \, p_{ij}, \qquad \text{(Equation 2)}$$

where $\boldsymbol{W}_{ij}^{\mathrm{CT}}$ denotes the synaptic weight from thalamic unit j onto cortical unit i, and $\boldsymbol{B} \in \mathbb{R}^{N\times R}$ denotes random feedback pathway weights that project the error $\boldsymbol{\varepsilon}_t$ back into the cortical network for learning. The eligibility trace p_{ij} reflects the correlation between recent activity of the thalamic unit j and the cortical unit i: $\tau \dot{p}_{ij} = -p_{ij}(t) + \varphi'(u_i(t))r_j(t)$, where u_i denotes the membrane potential of the i^{th} cortical neuron. Readout weight updates follow a standard delta-rule, $\delta \boldsymbol{W}_{ij}^{\mathrm{O}} \propto \varepsilon_i(t) h_j(t)$, where $\varepsilon_i(t)$ denotes the error in the i^{th} output dimension. Like other three-factor rules,[46] the update rule for thalamocortical synapses depends only on the presynaptic activity (thalamic neuron), the postsynaptic activity (cortical neuron), and the error signal at each moment (STAR Methods). Evidence for error signals in the superficial layers of the cortex[47,48] suggests that thalamocortical synapses located on apical dendrites (e.g., Guo et al.[5]) are particularly good candidates for this learning rule. Alternatively, error signals conveyed to apical dendrites could also drive plasticity in basal thalamocortical synapses via dendritic plateau potentials.[49,50] While recent computational models propose to take advantage of error signals in apical dendrites to approximate backpropagation,[51–53] here we restrict our focus to the three-factor learning rule described above.

We quantified the performance of models trained by applying the above learning rule as $1 - R^2$, where R^2 denotes the fraction of variance in the target function (a complex temporal waveform) that is predicted by the readout at the end of thalamocortical learning. We found that the performance improves with the number of thalamic neurons, suggesting that local plasticity at thalamocortical synapses ($\boldsymbol{W}^{\mathrm{CT}}$) facilitates learning (Figure 1C, green). This improvement in learning performance is accompanied by an increase in the alignment between weights in the feedback pathway $\mathbf{B}$ (which communicate error signals to post-synaptic neurons) and readout weights $\mathbf{W}^{\mathrm{O}}$ (Figure 1D, green), indicating that the learning rule performs credit assignment—conveying appropriate learning signals to neurons upstream of behavioral output—in thalamocortical synapses. Nonetheless, the performance of this learning strategy may depend critically on the signal received by thalamic neurons via corticothalamic projections ($\boldsymbol{W}^{\mathrm{TC}}$, Figure 1B, black).

Studies of biologically plausible algorithms in recurrent neural networks have typically dealt only with the learning of synapses onto neurons that are directly connected to the readout.[39,54–56] Since corticothalamic synapses are further upstream than thalamocortical synapses, it is not known whether biologically plausible plasticity rules can perform credit assignment in these synapses. Lack of empirical support for plasticity in corticothalamic synapses notwithstanding, we wanted to know whether this is possible in principle. To test this, we assume that the error signals are also communicated to the thalamus through a different set of feedback pathway weights, $\mathbf{B}'$. We trained our model by applying a local plasticity rule analogous to Equation 2 to update corticothalamic synapses (STAR Methods, Equation 6; Figure S1A). Successful learning in these synapses is a more challenging proposition as it requires good alignment between feedback weights $\mathbf{B}'$ and the *effective* readout weights of thalamic neurons (given by $\boldsymbol{W}^{\mathrm{O}}\boldsymbol{W}^{\mathrm{CT}}$ in a linear approximation) to be established through learning. In contrast to models that learn by updating only thalamocortical synapses, local plasticity operating simultaneously at thalamocortical and corticothalamic synapses does not yield any improvement in learning performance over what is obtained from learning only thalamocortical synapses with fixed random corticothalamic connections (Figure 1C, gray vs. green).

The failure of local plasticity in corticothalamic synapses to improve performance can be understood by comparing the feedback alignment of neurons in the cortex and thalamus. Whereas local plasticity achieves a high level of feedback alignment in cortical neurons, the alignment is no greater than chance in thalamic neurons (Figure 1D, black vs. green). Therefore, error signals are unable to mediate learning via standard three-factor plasticity rules in corticothalamic synapses (Figures S1B and S1C). One way to overcome this challenge is to initialize thalamocortical weights to have small ($\sim O(1/N)$) variance such that thalamic influence on cortical activity is minimal prior to learning (Figure S1D). However, this implies an experience-dependent

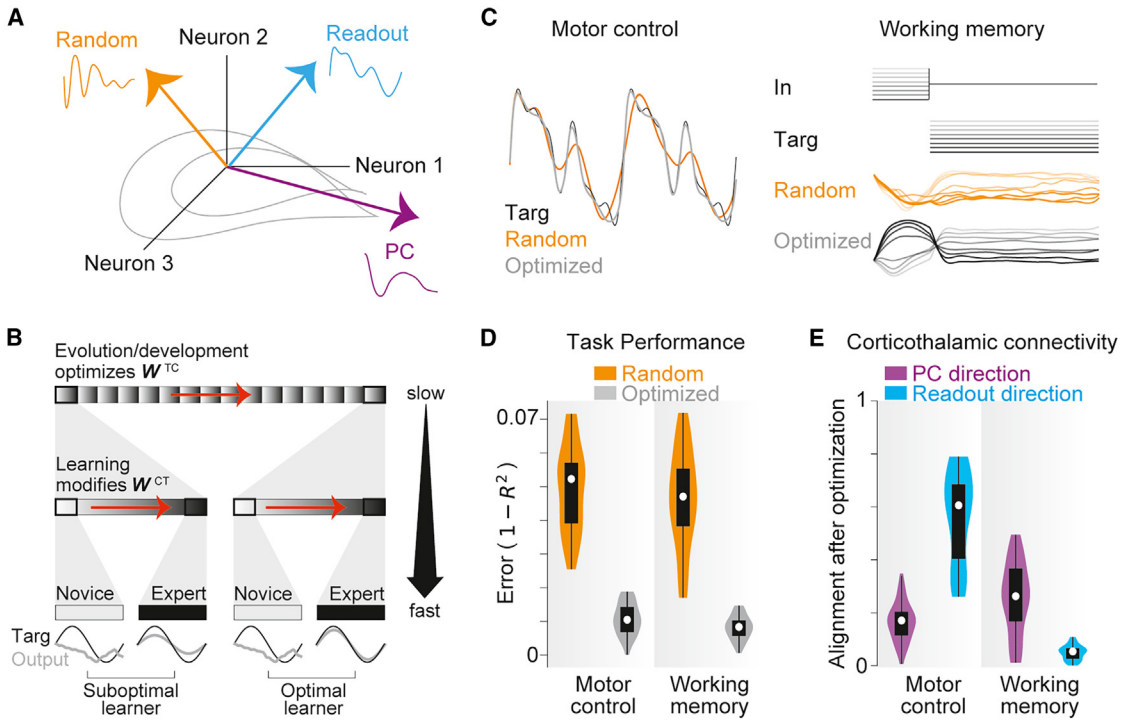

Figure 2. Corticothalamic connectivity optimized by meta-learning

(A) Corticothalamic weights may prioritize communicating specific subspaces of cortical activity, such as the readout (cyan) or principal component directions (purple), in contrast to a random subspace (orange).

(B) Schematic of the meta-learning procedure. Optimizing corticothalamic weights on a slow timescale (top, "outer loop") improves error-driven learning in thalamocortical synapses (middle, "inner loop"), improving performance (bottom).

(C) Left: median outputs (across simulations) of networks trained using meta-learned corticothalamic weights (gray) and random corticothalamic weights (orange), on the autonomous control task. The black line denotes the target function. Right: inputs and outputs of networks trained using meta-learned corticothalamic weights (gray) and random corticothalamic weights (orange) for the different conditions of the working memory task.

(D) Performance error ($1 - R^2$) of the model (across simulations initialized with different thalamocortical weights) trained using the meta-learned corticothalamic weights (gray), compared with the performance error of the model trained using random corticothalamic weights (orange).

(E) Alignment of meta-learned corticothalamic weights with the readout direction (cyan) and the direction of the leading principal component of cortical activity (purple) in the two tasks. White dots denote the median, black boxes denote interquartile range and black lines denote adjacent values. All models have $N = 256$ cortical neurons and $M = 32$ thalamic neurons. See also Figure S2.

increase in thalamic control of cortical activity dynamics and biological mechanisms that restrict learning to synapses that are initially weak, assumptions that await experimental validation. Therefore, here we restrict our focus to models with strong initial thalamocortical weights.

Optimal corticothalamic connectivity improves learning performance

Since biologically plausible feedback-driven plasticity has limited potential to optimize corticothalamic connectivity, we asked whether other mechanisms could select patterns of synaptic weights that improve performance. In particular, we sought to identify subspaces of cortical activity that, when communicated to the thalamus, improve learning supported by thalamocortical plasticity (Figure 2A). Specific corticothalamic connectivity that routes activity in such subspaces may be established by evolutionary or developmental processes,[57] or by plasticity rules of a different form than Equation 2.

To begin, we took an approach known as meta-learning or "learning to learn."[40,41] Corticothalamic weights were optimized at a longer timescale across thousands of epochs ("outer loop"), each of which comprises a few hundred trials of thalamocortical learning ("inner loop"; Figure 2B; STAR Methods). The outer loop represents the evolutionary or developmental processes that optimize corticothalamic connectivity. Optimization was performed via backpropagation through time (BPTT). To ensure that corticothalamic weights discovered by this technique did not depend on the precise state of thalamocortical weights at the beginning of learning, we reset the thalamocortical weights at the beginning of each epoch. Moreover, to ensure that this technique promotes learning specifically via thalamocortical synapses, we fixed all other weights, and enforced feedback alignment ($\boldsymbol{B}^{\mathrm{T}} = \boldsymbol{W}^{\mathrm{O}}$) during the meta-learning procedure. We later relax these constraints and test our conclusions in a model with plasticity in corticocortical and readout weights. To test the learning performance, we train the thalamocortical weights in the model using the fixed, optimized corticothalamic weights and compare the performance against a model trained using fixed random corticothalamic weights (STAR Methods).

Which corticothalamic projections are most suitable for thalamocortical learning could depend on the task. To test this hypothesis, we consider two prototypical neuroscience tasks with distinct computations—an autonomous motor control task and a working memory task. The goal of the autonomous control task is to output a complex temporal waveform without the aid of external inputs (i.e., analogous to the EMG activity required for internally generated movement). The goal of the working memory task is to output the amplitude of one of eight possible transient input pulses during a subsequent delay period (STAR Methods). We optimized corticothalamic weights for each task as outlined above, and found that meta-learned corticothalamic weights substantially improved learning supported by thalamocortical weights in both tasks (Figure 2C). The error dropped severalfold across both tasks when thalamocortical learning was performed using optimized corticothalamic weights as opposed to random corticothalamic weights (Figure 2D; median factor of reduction in error: motor control, 5.8; working memory, 5.1). We found qualitatively similar results when learning in the presence of random error-feedback weights, $\boldsymbol{B}$ (STAR Methods; Figure S2A), showing that the improvement in learning performance cannot be attributed to feedback alignment used in the meta-learning procedure.

We next sought to understand what structure in the optimized corticothalamic weights led to improved performance. We calculated the alignment β between the optimized corticothalamic weights and both the direction with the highest variance (principal-component direction) and the direction that drives output (readout direction) (STAR Methods; Figure 2E). We express the alignment in a normalized scale $(\beta - \beta_0)/(1 - \beta_0)$, where β_0 corresponds to the average alignment between meta-learned corticothalamic weights and a random direction in the cortical activity space. Whereas alignment with the readout direction was significantly greater than the alignment with the leading PC in the motor control task ($p = 1.6 \times 10^{-4}$, paired t test), this pattern was inverted for the working memory task where in fact the corticothalamic weights were more strongly aligned with the direction of the leading PC ($p = 2.8 \times 10^{-3}$, paired t test, Figure 2E). Pre-aligning corticothalamic weights to the readout direction at the beginning of the meta-learning procedure did not alter these results (Figure S2B). Together, these results demonstrate a nontrivial interplay between corticothalamic structure and task demands. Specifically, corticothalamic projections promote learning of autonomous control largely by communicating the cortical output to the thalamus, while learning of working memory benefits from communicating the PCs of the cortical activity to the thalamus.

Subspace-aligned corticothalamic connectivity outperforms random corticothalamic projection

The above analyses suggest that alignment of corticothalamic weights with specific subspaces of cortical activity improves performance. To directly test whether these subspaces are able to support learning by themselves, we consider three idealized models with categorically different forms of corticothalamic connectivity that correspond to varying degrees of structure (STAR Methods; Figure 2B). First, we consider unstructured connectivity that carries a *random subspace* of the cortical activity. Then, we consider connectivity aligned with the leading *principal components* (PCs) of cortical activity. Finally, we consider corticothalamic connectivity that is aligned with the *readout direction* and thus transmits a copy of the network output to the thalamus.

We first trained the above models separately on both tasks by assuming maximum corticothalamic compression ($M = 1$). We found that learning thalamocortical synapses from a single thalamic neuron is sufficient to perform the tasks provided the corticothalamic projection onto that neuron is chosen appropriately. For autonomous control, aligning corticothalamic connectivity with the readout direction yielded a substantial improvement over other strategies (Figure 3A). In contrast, the working memory task benefited from aligning corticothalamic connectivity to the leading PC of cortical activity (Figure 3B). These results are consistent with the structure of corticothalamic weights when optimized by meta-learning for each task (Figure 2E).

Models with a single thalamic neuron represent an extreme scenario in which only a one-dimensional subspace of cortical activity supports learning. We therefore asked how our results change for higher-dimensional corticothalamic projections. We tested this by training the variants of the above models with different numbers of thalamic neurons M. When aligning corticothalamic connectivity with the readout subspace, the remaining $M - 1$ thalamic neurons receive random projections. When corticothalamic connectivity is aligned with PCs, each thalamic neuron receives one of the M leading PCs of cortical activity. The performance of all models gradually improved with the number of thalamic neurons (Figures 3C and 3D). This makes sense because an increasingly larger subspace of cortical activity participates in learning, as we approach the limit where there would be no compression ($M = N$). Nonetheless, the advantage of aligning corticothalamic projections with the readout direction (for autonomous control; Figure 3C) or PC directions (for working memory; Figure 3D) persists even when M is relatively large, demonstrating that structured connectivity is beneficial for realistic ratios of thalamic to cortical neurons.

To verify that the relative performance of different corticothalamic structures is governed by the type of task and not the level of complexity, we trained the models on variants of both types of tasks at different levels of complexity (STAR Methods). We found that the choice of corticothalamic structure that maximized learning depends only on the type of task being learned and not on task complexity (Figures 3E and 3F). An exception is when the tasks are made too simple, where performance is substantially better than random regardless of whether the corticothalamic structure is aligned with the PC direction or the readout direction (median factor of reduction in error relative to random connectivity: motor control task, PC-aligned, 2.6; readout-aligned, 2.7; working memory task, PC aligned, 3.8×10^3; readout aligned, 6.1×10^4). Notably, even for the simplest task variants, models with random corticothalamic connectivity learn poorly.

In the models considered so far, we made two simplifying choices. First, they comprise a fixed small number ($N = 256$) of cortical neurons. It is unclear whether the benefit of structured corticothalamic projections for learning generalizes to larger networks. Second, we assume that the optimized or subspace aligned corticothalamic projections target just one of the neurons in the thalamus. In contrast, it has been argued that brain networks

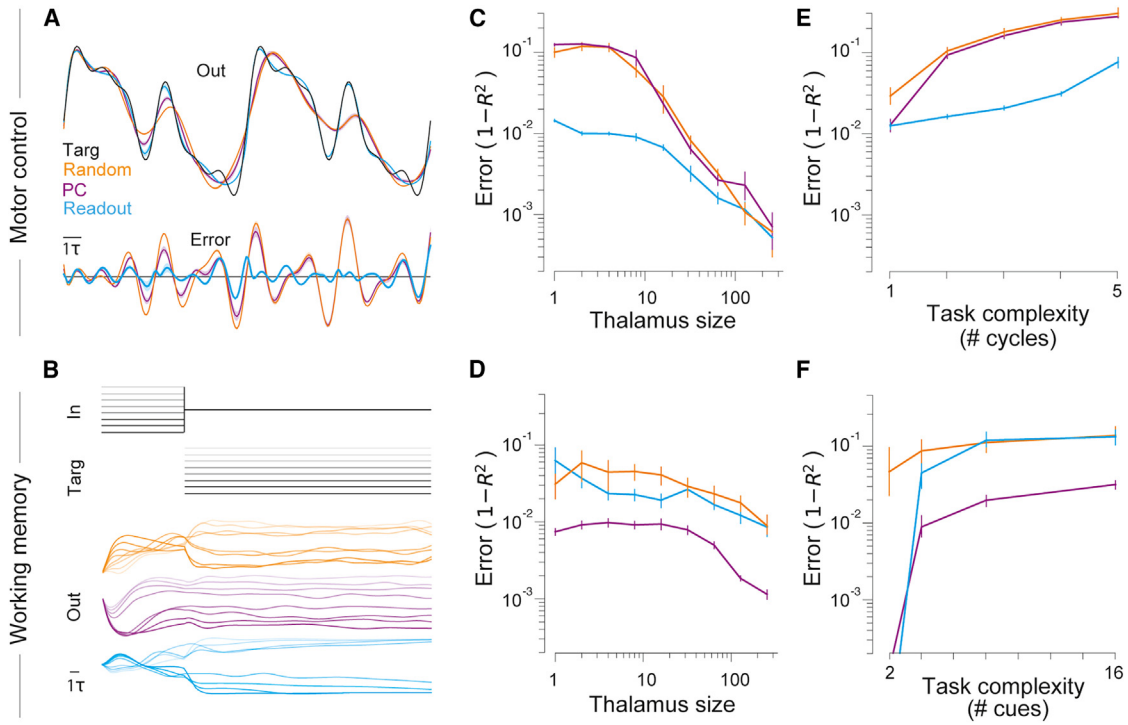

Figure 3. Different corticothalamic structures support different tasks

(A) Top: median outputs (across simulations) of networks with a single thalamic unit ($M = 1$) and different corticothalamic connectivity, trained on the autonomous control task. Bottom: the deviation of the output from the target function. Black dashed line denotes the target function.

(B) Network inputs and outputs for eight different conditions of the working memory task.

(C) Median performance of models with different numbers of thalamic units, M. Lower values of $1 - R^2$ correspond to better performance.

(D) Similar to (C), but for the working memory task.

(E) Median performance as a function of task complexity (STAR Methods).

(F) Similar to (E), but for the working memory task. All models have $N = 256$ cortical units. Error bars denote standard errors estimated by bootstrapping.

employ a coding scheme in which signals are distributed across a neural population.[58–60] To extrapolate to more realistic settings, we performed simulations by relaxing both choices (STAR Methods). We found that the performance benefit of learning by preferentially aligning the corticothalamic projections with the directions identified above was stable across different sizes of the cortical network (Figures 4A and 4B). The results were also not strongly dependent on the size of the thalamus: decreasing the compression ratio from 100 to 10 produced only a modest drop in the performance benefit (Figures 4A and 4B, solid vs. dashed), suggesting that the results are valid for the range of corticothalamic compression factors found across species.[42] Furthermore, in both tasks, we found that corticothalamic connectivity that communicates a fraction of variance in the activity from the cortical subspaces identified above was sufficient to produce an improvement in learning performance (Figures 4C and 4D).

To understand why the relationship between corticothalamic structure and learning performance is task dependent, we examined the PCs of the cortical dynamics in both tasks. In the autonomous motor control task, the temporal fluctuations of the leading PCs tend to be very slow (Figure S3A). Communicating signals in this subspace to the thalamus cannot support learning because these signals are not adequate to generate the high-frequency components in the target function. In contrast, the leading PCs of the cortical activity in the working memory task are dominated by the transient external inputs, and therefore encode the identity of the input (Figure S3B). Projecting these signals to the thalamus allows thalamocortical synapses to facilitate learning by contributing to building persistent activity (reflected in the gradual decrease in dimensionality of cortical activity; Figure S3D) that encodes stimulus identity during the subsequent delay period. Accordingly, the leading PCs are substantially aligned with the readout direction in the model trained on this task (Figure 4E, blue). In contrast, the readout direction in the model trained on motor control is mostly aligned with cortical PCs characterized by high frequency fluctuations, which have low variance (Figures 4E, red, and S5I). Furthermore, the readout shifts toward PCs with even lower variance as the task complexity is increased (Figure S3C) since modes containing high frequencies needed to support complex movement patterns tend to have low variance with few exceptions.[61] This difference in the readout profile between tasks implies that fewer cortical PCs are needed to explain the activity of thalamic neurons participating in working memory tasks compared with motor control (Figure 4F). We later show that neural activity in the mouse thalamus is consistent with these predictions.

Taken together, these results highlight the need for communicating signals from specific subspaces via corticothalamic projections and suggest that the subspace of cortical activity

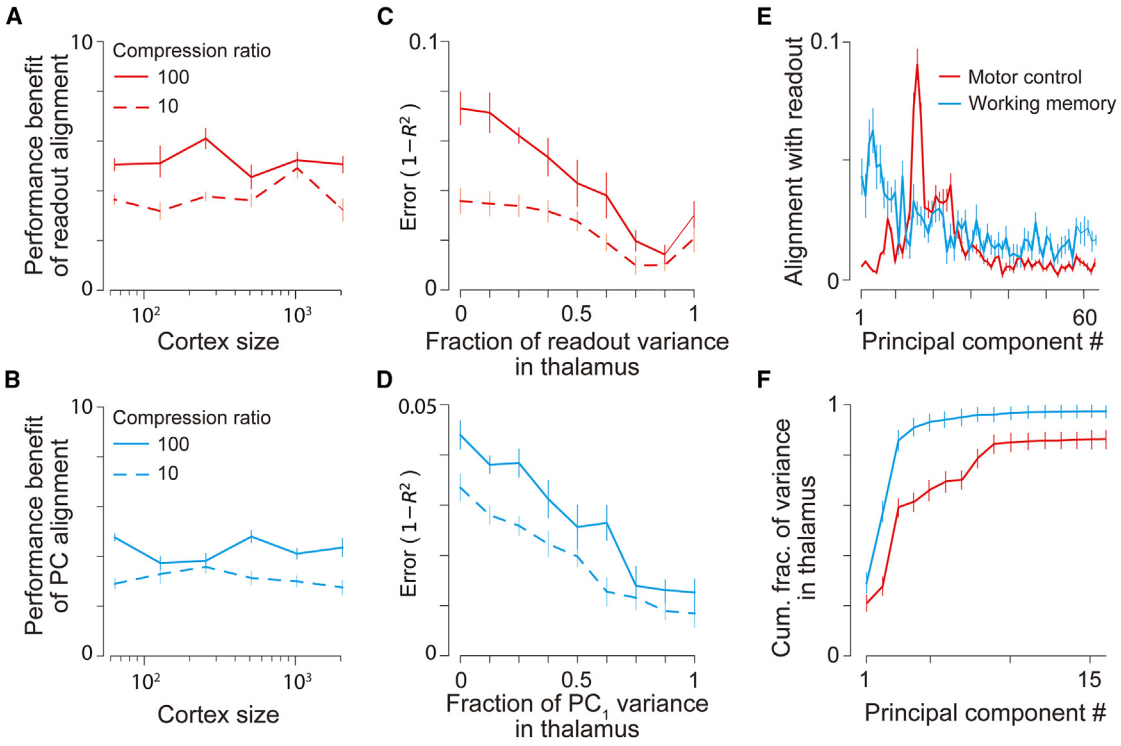

Figure 4. Findings generalize to larger models with distributed thalamic representation

(A) Performance benefit of aligning corticothalamic weights with the readout direction over aligning with a random subspace for motor learning, as a function of the size of the cortical population up to $N = 2{,}048$. It is quantified as $(1 - R_0^2)/(1 - R^2)$, where R_0^2 is the fraction of variance in the target function predicted by the output of a model that uses random corticothalamic weights (a value of 1 corresponds to no benefit). Solid and dashed lines correspond to models with two biologically plausible choices of compression ratio, N/M.

(B) Similar to (A), but demonstrating the performance benefit of aligning with the leading principal component (PC) of the cortex for learning of working memory.

(C) Median learning performance in the motor control task as a function of the fraction of variance in the readout direction communicated to the thalamic population for $N = 2{,}048$.

(D) Learning performance in the working memory task as a function of the fraction of variance in the leading PC of the cortex communicated to the thalamic population for $N = 2{,}048$.

(E) Alignment of different cortical PCs (sorted by variance, high to low) with the readout direction for motor control (red) and working memory (blue) tasks.

(F) Cumulative variance in the activity of thalamic neurons explained by the leading cortical PCs. (E and F) Correspond to a compression ratio of 100. Error bars denote ± 1 SEM estimated by bootstrapping. See also Figure S3–S5.

to which thalamic neurons should be tuned is task dependent. The benefits of optimized corticothalamic connectivity are not observed unless thalamocortical synapses are learned (Figures S4A and S4B). This suggests that performance cannot be improved if thalamus simply relays the activity in this subspace. Instead, structured corticothalamic connectivity improves task performance by enabling thalamocortical learning. Moreover, we found that structure in the corticothalamic connectivity is useful even if this structure is established gradually in conjunction with the learning of thalamocortical synapses (Figures S4C and S4D). Thus, learning is facilitated regardless of whether the corticothalamic connectivity is developmentally hardwired (as for efferent copies of signals to the motor periphery) or via activity-dependent mechanisms such as Hebbian learning (as for projections of the PCs of cortical activity). Furthermore, in contrast to a reservoir network where learning is limited to readout weights, the model with thalamocortical learning is more robust to noise in the initial activity state of the cortex (Figures S4E and S4F).

We sought to determine the conditions under which structured corticothalamic connectivity confers an advantage to thalamocortical learning by relaxing some modeling assumptions. First, we found that, when plasticity in thalamocortical synapses is implemented by BPTT instead of a three-factor rule (RFLO), the structure of corticothalamic weights does not influence the learning performance substantially (Figures S5A and S5B). This implies that structure specifically benefits simple thalamocortical learning algorithms by allowing them to operate on an appropriate neural representation. Second, we found that, even when thalamocortical plasticity is implemented by RFLO, the benefit of corticothalamic structure is dampened in the presence of recurrent excitatory connections between thalamic neurons (Figures S5C and S5D). Together with the effect of compression size on performance described above (Figures 4A and 4B, solid vs. dashed), this suggests that the connectivity constraints identified in this study apply to brain areas with properties that are characteristic of the thalamus—fewer neurons relative to the cortex and a lack of local recurrent excitation. Third, models in

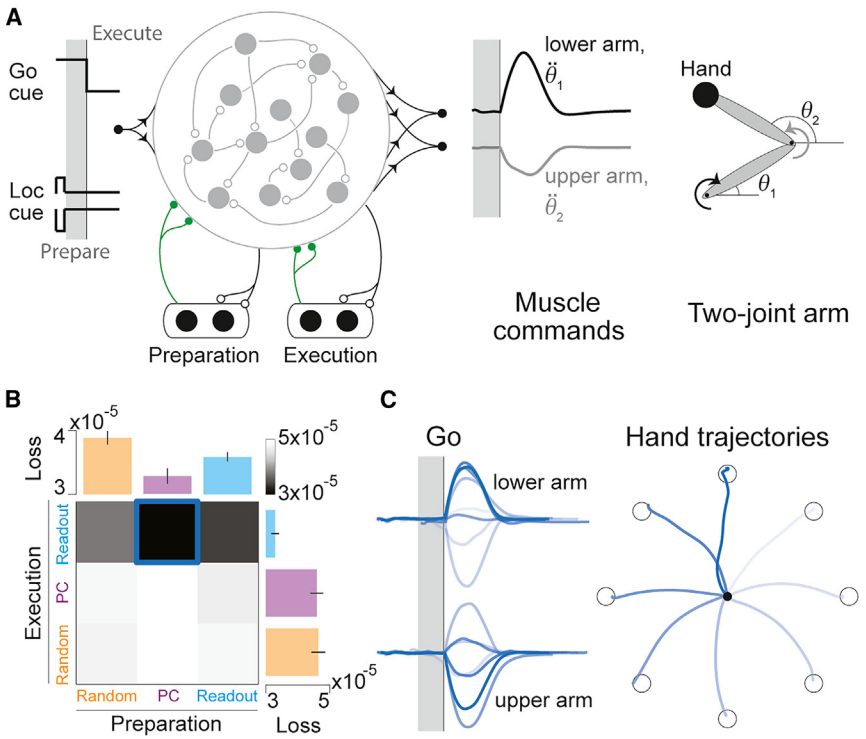

Figure 5. Thalamocortical model of goal-directed reaching

(A) The model comprises two thalamic modules, one of which is active only during movement preparation (time periods shaded in gray) and the other only during movement execution. The 2D output of the network controls the angular accelerations of the links of a two-joint arm.

(B) Performance of models with different types of corticothalamic connectivity onto preparatory and execution thalamic modules. Median performance of the best models from each row and column are shown in the bar plots.

(C) Left: outputs of the best model (blue square in B) for eight different reach conditions, shown in different shades of blue. Right: hand trajectories (center-out) corresponding to the outputs shown on the left. Open circles show target locations. Error bars denote standard errors. See also Figure S5.

which corticothalamic weights are updated using BPTT outperform other models (Figures S5E and S5F), suggesting that the structured corticothalamic weights are useful insofar as sophisticated plasticity mechanisms do not exist within the thalamus. Finally, we found that models with structured corticothalamic weights outperform random models even in the presence of corticocortical learning provided the latter is slow relative to thalamocortical learning (Figures S5G and S5H).

Findings generalize to composite motor/memory task

We have seen that different patterns of corticothalamic compression benefit autonomous control and working memory. However, naturalistic tasks often require both computations. To test whether our results generalize to such settings, we consider a delayed reaching task that combined aspects of working memory and motor control.[62] In this task, the model is required to execute reaching movements to a transiently cued location in a two-dimensional space represented on a screen. However, the movement can be initiated only upon the arrival of a go cue that follows the location cue after a random delay. Although the learning objective is solely a function of action and does not explicitly promote working memory, success in this task depends both on the ability to remember the target location during the delay (working memory) and the ability to execute movements in the absence of visual feedback (autonomous control). Therefore, we hypothesized that performance would be improved when different cortical subspaces are communicated to the thalamus during the delay and movement periods. Specifically, we hypothesized that learning benefits from communicating the PC directions during the delay period vs. the readout direction during the movement period.

To test this, we considered a thalamocortical model in which a cortical network is reciprocally connected to two distinct thalamic nuclei that are active either during preparation or execution (STAR Methods; Figure 5A). This architecture is motivated by recent experiments, which show that distinct populations of thalamic neurons are active before and during movement.[63] Due to the two-dimensional nature of this task, we considered a minimal model in which thalamic nuclei have two neurons each ($M = 2$). The cortex receives transient input pulses whose amplitudes encode one of eight possible target locations and a binary input, which serves as the go signal. The goal is to generate a pair of temporal waveforms that correspond to torques applied to the links of a two-joint arm, such that the endpoint of the arm reaches the target location (STAR Methods). We systematically varied the structure of corticothalamic connectivity onto both thalamic nuclei to select between a random subspace, leading PCs, or readout directions. Thalamocortical synapses were trained with RFLO. Consistent with our hypothesis, maximal performance was obtained in a model that conveyed PCs and readout signals to the thalamic nucleus that engaged in learning during preparation and execution, respectively (Figure 5B). This model exhibited excellent reaching performance to all targets (Figure 5C). The results were unchanged as we varied the number of target locations or the distribution of delays (Figure S5J). These results suggest that thalamocortical learning allows the cortex to perform different movements over a range of realistic delays, provided the corticothalamic structure is chosen appropriately.

Data are consistent with model predictions

Two recent studies in rodents used a combination of neurophysiology and optogenetics to demonstrate that dexterous movement generation[14] and working memory[10] both depend on

interactions between the thalamus and the cortex. We wanted to know whether this dependence is consistent with structured corticothalamic interactions that are optimized for learning. Since our findings indicate that thalamocortical learning of movement and memory are optimized by distinct patterns of corticothalamic interactions, we reanalyzed data from both experiments to directly test whether thalamic activity during those tasks depends on the components of cortical activity predicted by our model.

In the first task,[14] neural recordings were performed in the motor cortex and motor thalamus while mice performed a reach-to-grasp movement to grab a food pellet (Figures 6A, left and S6A). In the second,[10] recordings were performed in the frontal cortex (specifically the anterior lateral motor cortex [ALM]), and the thalamus (specifically ventral medial [VM] and ventral anterior-lateral [VAL]) nuclei, while mice performed a delayed discrimination task to report the location of an object following a delay of $\sim$ 1.3 s after the object was removed (Figures 6B, left and S6B). We used a linear regression model to decode behavior (hand acceleration or choice depending on the task) and the activity of individual thalamic neurons, from the cortical population activity (Figures 6A and 6B, right; STAR Methods). This technique identifies which modes of cortical activity propagate to behavior (i.e., estimate of readout weights, $\mathbf{W}^{O}$) and to the thalamus (estimate of corticothalamic weights, $\mathbf{W}^{TC}$). We restricted our analyses to the movement period and delay period for the motor control and working memory task, respectively.

We found that behavior was well explained by cortical activity in both tasks (R^2—motor control, 0.93; working memory, 0.97). To determine specifically which directions of cortical activity correlate with these behaviors, we examined the alignment of the readout weights with the PCs of cortical activity. In mice performing the working memory task, leading PCs of the frontal cortex activity had a large influence on the animal's behavioral choice (Figure 6C, blue). In contrast, hand movements during the motor task were primarily influenced by PCs of lower variance in the motor cortex (Figures 6C, red, and S6C). This difference is consistent with our model results and suggests that the PCs of the cortex that drive behavior are different for the two tasks.

Due to the greater contribution of lower variance PCs to the behavioral readout in the motor control task, we can test the key model prediction pertaining to the structure of corticothalamic connectivity—namely whether the structure is optimized for learning each task. Specifically, we predict that corticothalamic weights should be aligned with readout weights in the motor control task. This means that we would need lower variance PCs of cortical activity to capture the response of neurons in the thalamus (Figure 4F, red). In contrast, in the working memory task, we predict that corticothalamic weights should extract the leading PCs of cortical activity (Figure 4F, blue). If this is the case, we should be able to capture thalamic responses using only the high-variance PCs in the working memory task. Alternatively, our predictions would be violated if the leading cortical PCs do not capture more thalamic variance in the working memory task. We first quantified the fraction of variance explained (R^2) in each thalamic neuron when using the activity of all neurons recorded in the cortex (STAR Methods). We found that we could capture a substantial fraction of thalamic variance in both tasks, although the fraction was higher in the working memory task (motor control, 0.46 ± 0.01; working memory, 0.70 ± 0.01; Figure S6D). We then repeated this analysis to compute the fraction of variance explained in each thalamic neuron when using only the k leading PCs of cortical activity ($R^2(k)$). To compare corticothalamic interactions across the two tasks, we computed the fraction of *explainable* variance as a function of the number of PCs, $R^2(k)/R^2$. Consistent with the model prediction (Figures 4E and 4F), we found that more PCs are needed to explain thalamic activity during the motor control task than in working memory task (Figures 6D, red vs. blue, S6E, and S6F). The fraction of explainable variance in thalamus captured by the top 5 cortical PCs was significantly greater during the working memory task than motor control (motor control, 0.29 ± 0.02; working memory, 0.63 ± 0.04).

In the working memory task, inhibiting the cortex dramatically reduces variability in the thalamus, indicating that the interactions identified above are causal.[10] Similar inactivation experiments were not performed in the motor control task, but we took advantage of the fact that neural recordings were simultaneous to test whether trial-by-trial fluctuations in motor cortex propagate to the motor thalamus. We found that thalamic activity on any given trial was substantially better predicted by cortical activity in the same trial (Figure 6E, top), suggesting that the corticothalamic interactions do not merely reflect common inputs to motor cortex and thalamus. Furthermore, we found that corticothalamic weights that capture trial-by-trial activity in thalamic neurons were better aligned with the readout weights than those that capture only trial-averaged thalamic activity (Figure 6E, bottom). Therefore, fluctuations in corticothalamic signals across trials reflect fluctuations in the output of the motor cortex, suggesting that motor thalamus receives an efference copy of the motor command.

DISCUSSION

We developed a model of learning in thalamocortical networks by optimizing the structure of corticothalamic connectivity to support learning in thalamocortical synapses. We found that autonomous motor control requires a specialized corticothalamic pathway that communicates an efferent copy of the motor command, whereas the connectivity structure that projects the PCs of cortical activity facilitates working memory tasks. We analyzed neural recordings from the cortex and thalamus of mice during both types of tasks and found that the influence of the cortex on the thalamus is qualitatively consistent with these predictions.

Constraints on anatomy

We used meta-learning[40,41] to optimize corticothalamic weights while a local plasticity rule was applied to thalamocortical synapses. Similar approaches have recently been applied to other neural systems[65–67] and to identify biologically plausible learning rules.[68,69] Since this approach involves a slow optimization process based on gradient descent, in the context of our model the structure of the corticothalamic pathway identified in this manner is best viewed as a product of evolutionary and developmental

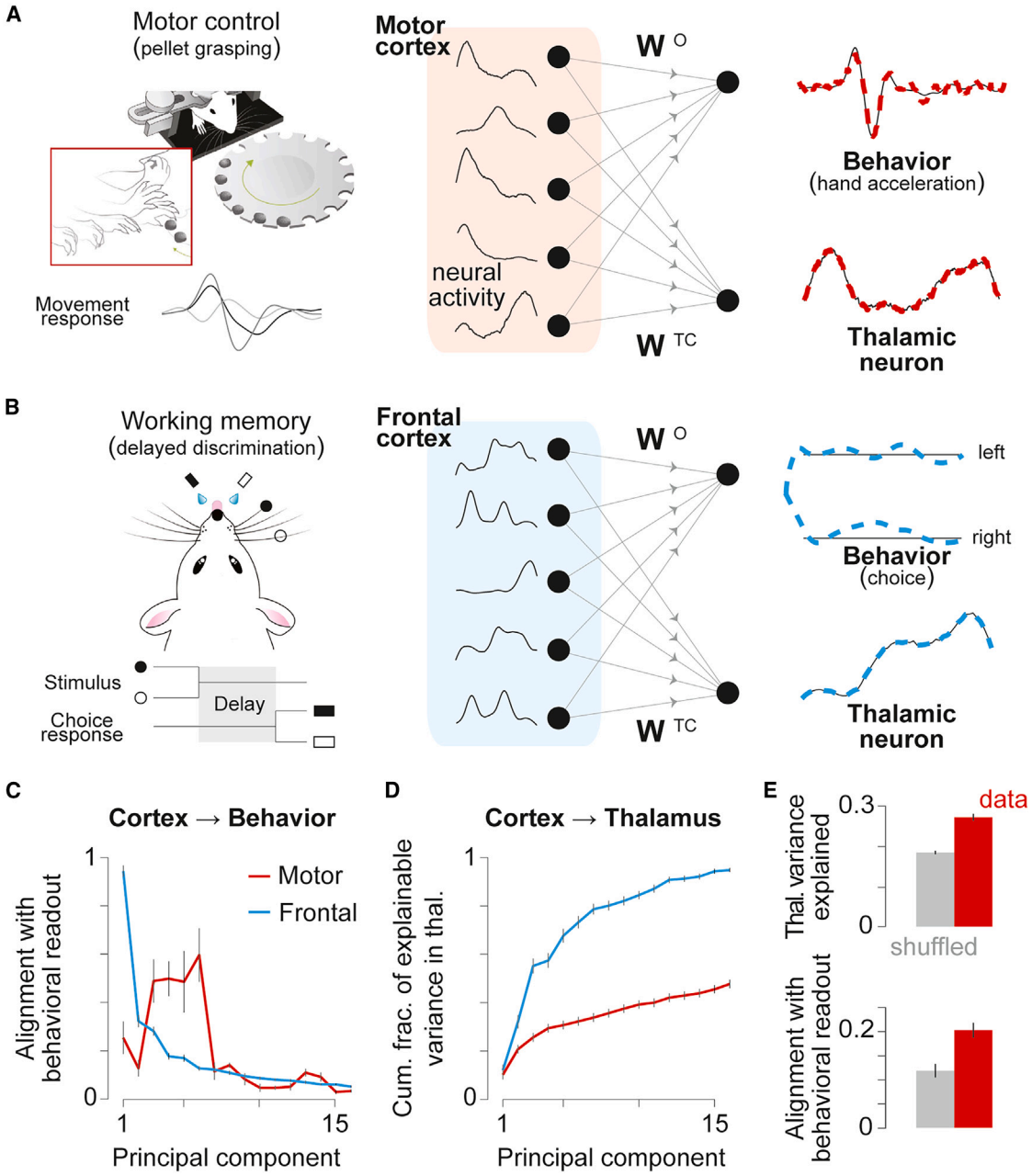

Figure 6. Corticothalamic interactions in mice are consistent with the model

(A) Left: motor control task—mice reached for a pellet of food following an acoustic cue, during recordings from the motor cortex and the motor thalamus. Right: regression of cortical activity against behavior (hand acceleration) and thalamic neuron activity, respectively. Traces show the activity of a subset of cortical neurons (middle panel), and decoded estimates of behavior and example of thalamic neuron activity (right panel; data in black and decoded estimate in color). Data were aligned to movement onset prior to regression.

(B) Left: working memory task, modified from Bjerre and Palmer[64]—mice reported the location of a pole by directional licking after a delay period, during recordings from the frontal cortex and thalamus. Right: regression of cortical activity against behavior (choice) and thalamic neuron activity. Data are aligned to the onset of delay period.

(C) Mean alignment between the direction of readout weights and different cortical PCs, in both tasks. Error bars denote ± 1 SEM. Motor control: n = 3 sessions; working memory: n = 5. Compare with model predictions in Figure 4E.

(D) Cumulative fraction of explainable variance in thalamic activity as a function of the number of cortical PCs. Fractions were normalized to a scale between 0 and 1 for each thalamic neuron before averaging. Compare with model predictions in Figure 4F.

(E) Top: fraction of variance in an average thalamic neuron explained by cortical PCs during the motor task. Bottom: average alignment between readout weights and corticothalamic weights across thalamic neurons. Red bars indicate single trial analyses; gray bars denote chance levels obtained by shuffling trial indices. Error bars in (D) and (E) denote standard errors in mean. Motor control: n = 101; working memory: n = 72. See also Figure S6.

processes. This view is consistent with a lack of clear evidence for plasticity in the corticothalamic pathway during learning, and supported by our finding that error-driven, biologically plausible learning algorithms are ineffective in adjusting corticothalamic synapses except when the network is initialized with small weights. While synapses in the cortex might undergo more sophisticated forms of plasticity by leveraging the complex dendritic machinery involving distinct apical and basal compartments,[49,70] such structures are absent in the thalamus and therefore cannot be used to perform credit assignment in corticothalamic synapses. It is possible that feedback pathways communicating error signals to the thalamus are themselves optimized by evolution and confer corticothalamic synapses with the potential for error-driven plasticity. Modeling studies have shown that such an approach is effective in the context of feedforward networks,[71–73] and would make for an interesting alternative hypothesis of learning in thalamocortical loops.

Anatomical tracing studies show that there is, indeed, an evolutionarily conserved pathway from layer V pyramidal neurons in the cortex to the higher-order thalamus through axonal branching of corticofugal projections.[74–78] Since a major target of corticofugal projections is lower motor centers such as the spinal cord, this pathway is ideally suited to convey an efference copy of the cortical motor output.[79,80] This is precisely the signal that would optimize thalamocortical learning of motor control according to our model. Our analysis of neural data confirmed that the alignment of the activity of thalamic neurons with the cortical motor output was significantly greater than chance during pellet grasping. While the degree of alignment was not perfect, we showed that learning with partial alignment is sufficient to facilitate learning (Figure S4C). Since the posterior region of the ventrolateral nucleus (VLp) is known to receive inputs from collateral axons in layer V of primary motor cortex,[81] it is a particularly good candidate for investigating motor learning.

For learning to maintain stimulus identity in working memory, we found that communicating the PCs of cortical activity to the thalamus is sufficient. This could be accomplished through unsupervised plasticity mechanisms that tune corticothalamic weights. Unlike error-based learning, unsupervised mechanisms such as Hebbian learning do not require credit assignment and can successfully operate on corticothalamic synapses.[82] This possibility is consistent with our analysis of neural data during the delayed discrimination task, which suggests that the corticothalamic pathway from the ALM to the VM/VAL complex communicates the PCs of activity in the ALM. While there is evidence for both Hebbian and homeostatic forms of plasticity in sensory thalamus,[83–86] evidence for plasticity in the higher-order thalamus is limited.[87] Our results identify the pathway from the ALM to the thalamus[5] as a leading candidate to investigate whether corticothalamic synapses undergo Hebbian plasticity, but we note that such mechanisms may be at play even in thalamic nuclei receiving motor efference copies.

Relationship to other studies

By accommodating experimental findings demonstrating an association between behavioral improvement and thalamocortical plasticity,[31–33,35] our model expands a body of work that conceptualizes connectivity in recurrent cortical networks as a sum of a random matrix and a tunable low-rank perturbation.[26,27,36,88] Our results suggest that changes in cortical representations observed during learning[89–91] may not be entirely due to plasticity of corticocortical synapses. While there is evidence for corticocortical plasticity that contributes to activity remapping observed during training,[33,92,93] we found that CTC loops can contribute substantially even in the presence of corticocortical plasticity. Therefore, thalamocortical and corticocortical plasticity play similar roles in our model, resulting in improved performance with increasing thalamic population size. This is in contrast to other systems where networks with bottlenecks outperform fully connected networks.[23] Determining the differential contribution of thalamocortical and corticocortical plasticity to learning is an important direction for future studies. One possibility is that different CTC loops are engaged in different contexts such that thalamocortical plasticity contributes to learning context-specific behavioral components whereas corticocortical plasticity helps consolidate components that are shared across contexts. Such coordination between cortex and thalamus is a potential solution to the problem of continual learning.[94]

Limitations of the study

In our models, thalamocortical synapses are updated according to a local plasticity rule for error-based learning.[39] There is also evidence for a role of dopamine in mediating cortical plasticity,[95,96] suggesting that reward-based learning rules may also modify thalamocortical synapses. The study does not address whether our results generalize to other forms of plasticity including spike-based algorithms.[56] Second, for simplicity, we used a coarse-grained model composed of a homogeneous neural populations in the cortex and thalamus. This overlooks experimental findings showing convergent inputs from multiple cortical areas to individual thalamic neurons,[97] rich heterogeneity in wiring across cortical layers that project to/from the thalamus,[7] and diversity in the membrane properties across thalamic neurons,[98] which may place additional constraints on computation in CTC loops. Finally, the thalamic reticular nucleus mediates local inhibition in the thalamus and alters its dynamical regime,[99] which we did not consider in our models.

Conclusion

Generic network architectures in which synaptic weights are trained end-to-end using, e.g., the backpropagation algorithm,[100–103] do not reveal how the brain makes use of specific anatomical circuit motifs and local plasticity rules to facilitate learning. We fill this gap in the context of CTC loops by demonstrating that task-specific, structured corticothalamic connectivity is necessary to optimize learning when biologically plausible plasticity rules are employed, thereby establishing a link between anatomy and computation. Our findings show that understanding the structure of corticothalamic connectivity may be key to determining the computational role of the higher-order thalamus in orchestrating behavior.

STAR★METHODS

Detailed methods are provided in the online version of this paper and include the following:

- KEY RESOURCES TABLE
- RESOURCE AVAILABILITY
  - Lead contact
  - Materials availability
  - Data and code availability
- METHOD DETAILS
  - Task description
  - Thalamocortical model
  - Learning algorithm
  - Subspace aligned models of corticothalamic connectivity
  - Models of distributed thalamic representation with partial subspace alignment of corticothalamic connectivity
- QUANTIFICATION AND STATISTICAL ANALYSIS
  - Task performance
  - Alignment between weights
  - Neural datasets
  - Estimation of readout weights
  - Analysis of corticothalamic communication

SUPPLEMENTAL INFORMATION

Supplemental information can be found online at https://doi.org/10.1016/j.celrep.2024.114059.

ACKNOWLEDGMENTS

K.J.L., M.X., A.L.-K., and S.E. were supported by NSF NeuroNex DBI-1707398 and Gatsby Charitable Foundation GAT3780. M.X. was supported by NIH T32-NS064929. J.D.C., B.A.S., and A.W.H. were supported by the HHMI. A.L.-K. was supported by the Burroughs Wellcome Fund. S.E. was supported by NIH U19 5U19NS104649, NIH CRCNS 5R01NS105349, and the Levy Foundation. We thank Guo et al.[10] for making their dataset publicly available.

AUTHOR CONTRIBUTIONS

K.J.L., M.X., A.L.-K., and S.E. developed the model. K.J.L. and M.X. performed the simulations. J.D.C., B.A.S., and A.W.H. performed the experiments and provided the data. K.J.L. analyzed the data. K.J.L., M.X., A.L.-K., and S.E. wrote the draft and all authors were involved in revising it.

DECLARATION OF INTERESTS

The authors declare no competing interests.

Received: May 22, 2023
Revised: January 4, 2024
Accepted: March 20, 2024

REFERENCES

1. Sherman, S.M. (2007). The thalamus is more than just a relay. Curr. Opin. Neurobiol. *17*, 417–422. https://doi.org/10.1016/j.conb.2007.07.003.
2. Murray Sherman, S., and Guillery, R.W. (2018). Exploring the Thalamus and its Role in Cortical Function (MIT Press). https://doi.org/10.7551/mitpress/2940.001.0001.
3. Guo, N.Y., Barrett, J.M., Tapies, M., and Shepherd, G.M.G. (2020). Cortico-thalamo-cortical circuits of mouse forelimb s1 are organized primarily as recurrent loops. J. Neurosci. *40*, 2849–2858. https://doi.org/10.1523/JNEUROSCI.2277-19.2020.
4. Yamawaki, N., and Shepherd, G.M.G. (2015). Synaptic circuit organization of motor corticothalamic neurons. J. Neurosci. *35*, 2293–2307. https://doi.org/10.1523/JNEUROSCI.4023-14.2015.
5. Guo, N.Y., Svoboda, K., and Shepherd, G.M.G. (2018). Anterolateral motor cortex connects with a medial subdivision of ventromedial thalamus through cell type-specific circuits, forming an excitatory thalamo-cortico-thalamic loop via layer 1 apical tuft dendrites of layer 5b pyramidal tract type neurons. J. Neurosci. *38*, 8787–8797. https://doi.org/10.1523/JNEUROSCI.1333-18.2018.
6. Economo, M.N., Viswanathan, S., Tasic, B., Bas, E., Winnubst, J., Menon, V., Graybuck, L.T., Nguyen, T.N., Smith, K.A., Yao, Z., et al. (2018). Distinct descending motor cortex pathways and their roles in movement. Nature *563*, 79–84. https://doi.org/10.1038/s41586-018-0642-9.
7. Muñoz-Castañeda, R., Zingg, B., Matho, K.S., Chen, X., Wang, Q., Foster, N.N., Li, A., Narasimhan, A., Hirokawa, K.E., Huo, B., et al. (2021). Cellular anatomy of the mouse primary motor cortex. Nature *598*, 159–166. https://doi.org/10.1038/s41586-021-03970-w.
8. Collins, D.P., Anastasiades, P.G., Marlin, J.J., and Carter, A.G. (2018). Reciprocal circuits linking the prefrontal cortex with dorsal and ventral thalamic nuclei. Neuron *98*, 366–379.e4. https://doi.org/10.1016/j.neuron.2018.03.024.
9. Bolkan, S.S., Stujenske, J.M., Parnaudeau, S., Spellman, T.J., Rauffenbart, C., Abbas, A.I., Harris, A.Z., Gordon, J.A., and Kellendonk, C. (2017). Thalamic projections sustain prefrontal activity during working memory maintenance. Nat. Neurosci. *20*, 987–996. https://doi.org/10.1038/nn.4568.
10. Guo, H.K.I., Daie, K., Druckmann, S., Gerfen, C.R., and Svoboda, K. (2017). Maintenance of persistent activity in a frontal thalamocortical loop. Nature *545*, 181–186. https://doi.org/10.1038/nature22324.
11. Schmitt, L.I., Wimmer, R.D., Nakajima, M., Happ, M., Mofakham, S., and Halassa, M.M. (2017). Thalamic amplification of cortical connectivity sustains attentional control. Nature *545*, 219–223. https://doi.org/10.1038/nature22073.
12. Rikhye, R.V., Gilra, A., and Halassa, M.M. (2018). Thalamic regulation of switching between cortical representations enables cognitive flexibility. Nat. Neurosci. *21*, 1753–1763. https://doi.org/10.1038/s41593-018-0269-z.
13. Alcaraz, F., Fresno, V., Marchand, A.R., Kremer, E.J., Coutureau, E., and Wolff, M. (2018). Thalamocortical and corticothalamic pathways differentially contribute to goal-directed behaviors in the rat. Elife *7*, e32517. https://doi.org/10.7554/eLife.32517.
14. Sauerbrei, B.A., Guo, J.Z., Cohen, J.D., Mischiati, M., Guo, W., Kabra, M., Verma, N., Mensh, B., Branson, K., and Hantman, A.W. (2020). Cortical pattern generation during dexterous movement is input-driven. Nature *577*, 386–391. https://doi.org/10.1038/s41586-019-1869-9.
15. Zhaoping, L. (2006). Theoretical understanding of the early visual processes by data compression and data selection. Network *17*, 301–334. https://doi.org/10.1080/09548980600931995.
16. Druckmann, S., Hu, T., and Chklovskii, D.B. (2012). A mechanistic model of early sensory processing based on subtracting sparse representations. Adv. Neural Inf. Process. Syst. *3*.
17. Olshausen, B.A., and Field, D.J. (1996). Emergence of simple-cell receptive field properties by learning a sparse code for natural images. Nature *381*, 607–609. https://doi.org/10.1038/381607a0.
18. Zhu, M., and Rozell, C.J. (2013). Visual nonclassical receptive field effects emerge from sparse coding in a dynamical system. PLoS Comput. Biol. *9*, e1003191. https://doi.org/10.1371/journal.pcbi.1003191.

19. Zhang, Y., and Sharpee, T.O. (2016). A robust feedforward model of the olfactory system. PLoS Comput. Biol. *12*, e1004850. https://doi.org/10.1371/journal.pcbi.1004850.

20. Qin, S., Li, Q., Tang, C., and Tu, Y. (2019). Optimal compressed sensing strategies for an array of nonlinear olfactory receptor neurons with and without spontaneous activity. Proc. Natl. Acad. Sci. USA *116*, 20286–20295. https://doi.org/10.1073/pnas.1906571116.

21. Babadi, B., and Sompolinsky, H. (2014). Sparseness and expansion in sensory representations. Neuron *83*, 1213–1226. https://doi.org/10.1016/j.neuron.2014.07.035.

22. Litwin-Kumar, A., Harris, K.D., Axel, R., Sompolinsky, H., and Abbott, L.F. (2017). Optimal degrees of synaptic connectivity. Neuron *93*, 1153–1164.e7. https://doi.org/10.1016/j.neuron.2017.01.030.

23. Muscinelli, S.P., Wagner, M.J., and Litwin-Kumar, A. (2023). Optimal routing to cerebellum-like structures. Nat. Neurosci. *26*, 1630–1641. https://doi.org/10.1038/s41593-023-01403-7.

24. Xie, M., Muscinelli, S., Harris, K.D., and Litwin-Kumar, A. (2023). Task-dependent optimal representations for cerebellar learning. Elife *12*, e82914. https://doi.org/10.7554/eLife.82914.

25. Ganguli, S., and Sompolinsky, H. (2012). Compressed sensing, sparsity, and dimensionality in neuronal information processing and data analysis. Annu. Rev. Neurosci. *35*, 485–508. https://doi.org/10.1146/annurev-neuro-062111-150410.

26. Kao, T.C., Sadabadi, M.S., and Hennequin, G. (2021). Optimal anticipatory control as a theory of motor preparation: A thalamo-cortical circuit model. Neuron *109*, 1567–1581.e12. https://doi.org/10.1016/j.neuron.2021.03.009.

27. Logiaco, L., Abbott, L.F., and Escola, S. (2021). Thalamic control of cortical dynamics in a model of flexible motor sequencing. Cell Rep. *35*, 109090. https://doi.org/10.1016/j.celrep.2021.109090.

28. Escola, G.S., Lakshminarasimhan, K., and Logiaco, L. (2023). Lakshminarasimhan, and Laureline Logiaco The Cerebral Cortex and Thalamus, chapter Models of Thalamocortical Interactions in Motor Control. Oxford Academic, 354–366. https://doi.org/10.1093/med/9780197676158.003.0034.

29. Herry, C., Rose, M.V., and Garcia, R. (1999). Plasticity in the mediodorsal thalamo-prefrontal cortical transmission in behaving mice. J. Neurophysiol. *82*, 2827–2832. https://doi.org/10.1152/jn.1999.82.5.2827.

30. Oberlaender, M., Ramirez, A., and Bruno, R.M. (2012). Sensory experience restructures thalamocortical axons during adulthood. Neuron *74*, 648–655. https://doi.org/10.1016/j.neuron.2012.03.022.

31. Biane, J.S., Takashima, Y., Scanziani, M., Conner, J.M., and Tuszynski, M.H. (2016). Thalamocortical projections onto behaviorally relevant neurons exhibit plasticity during adult motor learning. Neuron *89*, 1173–1179. https://doi.org/10.1016/j.neuron.2016.02.001.

32. Audette, N.J., Bernhard, S.M., Ray, A., Stewart, L.T., and Barth, A.L. (2019). Rapid plasticity of higher-order thalamocortical inputs during sensory learning. Neuron *103*, 277–291.e4. https://doi.org/10.1016/j.neuron.2019.04.037.

33. Hasegawa, R., Ebina, T., Tanaka, Y.R., Kobayashi, K., and Matsuzaki, M. (2020). Structural dynamics and stability of corticocortical and thalamocortical axon terminals during motor learning. PLoS One *15*, e0234930. https://doi.org/10.1371/journal.pone.0234930.

34. Adam, R., Schaeffer, D.J., Johnston, K., Menon, R.S., and Everling, S. (2021). Structural alterations in cortical and thalamocortical white matter tracts after recovery from prefrontal cortex lesions in macaques. Neuroimage *232*, 117919. https://doi.org/10.1016/j.neuroimage.2021.117919.

35. Sohn, J., Suzuki, M., Youssef, M., Hatada, S., Larkum, M.E., Kawaguchi, Y., and Kubota, Y. (2022). Presynaptic supervision of cortical spine dynamics in motor learning. Sci. Adv. *8*, eabm0531. https://doi.org/10.1126/sciadv.abm0531.

36. Mastrogiuseppe, F., and Ostojic, S. (2018). Linking connectivity, dynamics, and computations in low-rank recurrent neural networks. Neuron *99*, 609–623.e29. https://doi.org/10.1016/j.neuron.2018.07.003.

37. Schuessler, F., Mastrogiuseppe, F., Dubreuil, A., Ostojic, S., and Barak, O. (2020). The interplay between randomness and structure during learning in rnns. Adv. Neural Inf. Process. Syst. *33*, 13352–13362.

38. Dubreuil, A., Valente, A., Beiran, M., Mastrogiuseppe, F., and Ostojic, S. (2022). The role of population structure in computations through neural dynamics. Nat. Neurosci. *25*, 783–794. https://doi.org/10.1038/s41593-022-01088-4.

39. Murray, J.M. (2019). Local online learning in recurrent networks with random feedback. Elife *8*, e43299. https://doi.org/10.7554/eLife.43299.

40. Wang, J.X. (2021). Meta-learning in natural and artificial intelligence. Current Opinion in Behavioral Sciences *38*, 90–95. https://doi.org/10.1016/j.cobeha.2021.01.002.

41. Hospedales, T., Antoniou, A., Micaelli, P., and Storkey, A. (2022). Meta-learning in neural networks: A survey. IEEE Trans. Pattern Anal. Mach. Intell. *44*, 5149–5169. https://doi.org/10.1109/TPAMI.2021.3079209.

42. Halley, A.C., and Krubitzer, L. (2019). Not all cortical expansions are the same: the coevolution of the neocortex and the dorsal thalamus in mammals. Curr. Opin. Neurobiol. *56*, 78–86. https://doi.org/10.1016/j.conb.2018.12.003.

43. Arcelli, P., Frassoni, C., Regondi, M.C., De Biasi, S., and Spreafico, R. (1997). Gabaergic neurons in mammalian thalamus: A marker of thalamic complexity? Brain Res. Bull. *42*, 27–37. https://doi.org/10.1016/S0361-9230(96)00107-4.

44. Halassa, M.M., and Sherman, S.M. (2019). Thalamocortical circuit motifs: A general framework. Neuron *103*, 762–770. https://doi.org/10.1016/j.neuron.2019.06.005.

45. Tanaka, Y.H., Tanaka, Y.R., Kondo, M., Terada, S.I., Kawaguchi, Y., and Matsuzaki, M. (2018). Thalamocortical axonal activity in motor cortex exhibits layer-specific dynamics during motor learning. Neuron *100*, 244–258.e12. https://doi.org/10.1016/j.neuron.2018.08.016.

46. Gerstner, W., Lehmann, M., Liakoni, V., Corneil, D., and Brea, J. (2018). Eligibility traces and plasticity on behavioral time scales: Experimental support of neohebbian three-factor learning rules. Front. Neural Circ. *12*, 53. https://doi.org/10.3389/fncir.2018.00053.

47. Inoue, M., Uchimura, M., and Kitazawa, S. (2016). Error signals in motor cortices drive adaptation in reaching. Neuron *90*, 1114–1126. https://doi.org/10.1016/j.neuron.2016.04.029.

48. Heindorf, M., Arber, S., and Keller, G.B. (2018). Mouse motor cortex coordinates the behavioral response to unpredicted sensory feedback. Neuron *99*, 1040–1054.e5. https://doi.org/10.1016/j.neuron.2018.07.046.

49. Guerguiev, J., Lillicrap, T.P., and Richards, B.A. (2017). Towards deep learning with segregated dendrites. Elife *6*, e22901. https://doi.org/10.7554/eLife.22901.

50. Bittner, K.C., Milstein, A.D., Grienberger, C., Romani, S., and Magee, J.C. (2017). Behavioral time scale synaptic plasticity underlies ca1 place fields. Science *357*, 1033–1036. https://doi.org/10.1126/science.aan3846.

51. Sacramento, J., Costa, R.P., Bengio, Y., and Senn, W. (2018). Dendritic cortical microcircuits approximate the backpropagation algorithm. Adv. Neural Inf. Process. Syst. *31*.

52. Payeur, A., Guerguiev, J., Zenke, F., Richards, B.A., and Naud, R. (2021). Burst-dependent synaptic plasticity can coordinate learning in hierarchical circuits. Nat. Neurosci. *24*, 1010–1019. https://doi.org/10.1038/s41593-021-00857-x.

53. Greedy, W., Zhu, H.W., Pemberton, J., Mellor, J., and Costa, R.P. (2022). Single-phase deep learning in cortico-cortical networks. Adv. Neural Inf. Process. Syst. *35*, 24213–24225.

54. Miconi, T. (2017). Biologically plausible learning in recurrent neural networks reproduces neural dynamics observed during cognitive tasks. Elife *6*, e20899. https://doi.org/10.7554/eLife.20899.

55. Alemi, A., Denève, S., Machens, C.K., and Slotine, J.J. (2018). Learning nonlinear dynamics in efficient, balanced spiking networks using local plasticity rules. In 32nd AAAI Conference on Artificial Intelligence, AAAI 2018. https://doi.org/10.1609/aaai.v32i1.11320.

56. Gilra, A., and Gerstner, W. (2017). Predicting non-linear dynamics by stable local learning in a recurrent spiking neural network. Elife *6*, e28295. https://doi.org/10.7554/eLife.28295.

57. Zador, A.M. (2019). A critique of pure learning and what artificial neural networks can learn from animal brains. Nat. Commun. *10*, 3770. https://doi.org/10.1038/s41467-019-11786-6.

58. Averbeck, B.B., Latham, P.E., and Pouget, A. (2006). Neural correlations, population coding and computation. Nat. Rev. Neurosci. *7*, 358–366.

59. Barack, D.L., and Krakauer, J.W. (2021). Two views on the cognitive brain. Nat. Rev. Neurosci. *22*, 359–371. https://doi.org/10.1038/s41583-021-00448-6.

60. Ebitz, R.B., and Hayden, B.Y. (2021). The population doctrine in cognitive neuroscience. Neuron *109*, 3055–3068. https://doi.org/10.1016/j.neuron.2021.07.011.

61. Schuessler, F., Mastrogiuseppe, F., Ostojic, S., and Barak, O. (2023). Aligned and oblique dynamics in recurrent neural networks. Preprint at arXiv. https://doi.org/10.48550/arXiv.2307.07654.

62. Churchland, M.M., Cunningham, J.P., Kaufman, M.T., Foster, J.D., Nuyujukian, P., Ryu, S.I., Shenoy, K.V., and Shenoy, K.V. (2012). Neural population dynamics during reaching. Nature *487*, 51–56. https://doi.org/10.1038/nature11129.

63. Gaidica, M., Hurst, A., Cyr, C., and Leventhal, D.K. (2018). Distinct populations of motor thalamic neurons encode action initiation, action selection, and movement vigor. J. Neurosci. *38*, 6563–6573. https://doi.org/10.1523/JNEUROSCI.0463-18.2018.

64. Bjerre, A.S., and Palmer, L.M. (2020). Probing cortical activity during head-fixed behavior. Front. Mol. Neurosci. *13*, 30. https://doi.org/10.3389/fnmol.2020.00030.

65. Wang, Z.K.-N., Kumaran, D., Tirumala, D., Soyer, H., Leibo, J.Z., Hassabis, D., and Botvinick, M. (2018). Prefrontal cortex as a meta-reinforcement learning system. Nat. Neurosci. *21*, 860–868. https://doi.org/10.1038/s41593-018-0147-8.

66. Jiang, L., and Litwin-Kumar, A. (2021). Models of heterogeneous dopamine signaling in an insect learning and memory center. PLoS Comput. Biol. *17*, e1009205. https://doi.org/10.1371/journal.pcbi.1009205.

67. Tyulmankov, D., Yang, G.R., and Abbott, L.F. (2022). Meta-learning synaptic plasticity and memory addressing for continual familiarity detection. Neuron *110*, 544–557.e8. https://doi.org/10.1016/j.neuron.2021.11.009.

68. Confavreux, B., Zenke, F., Agnes, E.J., Lillicrap, T., and Vogels, T.P. (2020). A meta-learning approach to (re)discover plasticity rules that carve a desired function into a neural network. Adv. Neural Inf. Process. Syst. *33*, 16398–16408.

69. Shervani-Tabar, N., and Rosenbaum, R. (2023). Meta-learning biologically plausible plasticity rules with random feedback pathways. Nat. Commun. *14*, 1805. https://doi.org/10.1038/s41467-023-37562-1.

70. Urbanczik, R., and Senn, W. (2014). Learning by the dendritic prediction of somatic spiking. Neuron *81*, 521–528. https://doi.org/10.1016/j.neuron.2013.11.030.

71. Lee, D.-H., Zhang, S., Biard, A., and Bengio, Y. (2014). Target propagation. In International Conference on Learning Representations, *15*.

72. Akrout, M., Wilson, C., Humphreys, P.C., Lillicrap, T., and Douglas, T. (2019). Deep learning without weight transport. Adv. Neural Inf. Process. Syst. *32*.

73. Lindsey, J., and Litwin-Kumar, A. (2020). Learning to learn with feedback and local plasticity. Adv. Neural Inf. Process. Syst. *33*, 21213–21223.

74. Bourassa, J., Pinault, D., and Deschênes, M. (1995). Corticothalamic projections from the cortical barrel field to the somatosensory thalamus in rats: A single-fibre study using biocytin as an anterograde tracer. Eur. J. Neurosci. *7*, 19–30. https://doi.org/10.1111/j.1460-9568.1995.tb01016.x.

75. Bourassa, J., and Deschênes, M. (1995). Corticothalamic projections from the primary visual cortex in rats: a single fiber study using biocytin as an anterograde tracer. Neuroscience *66*, 253–263. https://doi.org/10.1016/0306-4522(95)00009-8.

76. Kakei, S., Na, J., and Shinoda, Y. (2001). Thalamic terminal morphology and distribution of single corticothalamic axons originating from layers 5 and 6 of the cat motor cortex. J. Comp. Neurol. *437*, 170–185. https://doi.org/10.1002/cne.1277.

77. Kita, T., and Kita, H. (2012). The subthalamic nucleus is one of multiple innervation sites for long-range corticofugal axons: A single-axon tracing study in the rat. J. Neurosci. *32*, 5990–5999. https://doi.org/10.1523/JNEUROSCI.5717-11.2012.

78. Sherman, S.M. (2016). Thalamus plays a central role in ongoing cortical functioning. Nat. Neurosci. *19*, 533–541. https://doi.org/10.1038/nn.4269.

79. Guillery, R.W., and Sherman, S.M. (2011). Branched thalamic afferents: What are the messages that they relay to the cortex? Brain Res. Rev. *66*, 205–219. https://doi.org/10.1016/j.brainresrev.2010.08.001.

80. Sherman, S.M., and Usrey, W.M. (2021). Cortical control of behavior and attention from an evolutionary perspective. Neuron *109*, 3048–3054. https://doi.org/10.1016/j.neuron.2021.06.021.

81. Bosch-Bouju, C., Hyland, B.I., and Parr-Brownlie, L.C. (2013). Motor thalamus integration of cortical, cerebellar and basal ganglia information: Implications for normal and parkinsonian conditions. Front. Comput. Neurosci. *7*, 163. https://doi.org/10.3389/fncom.2013.00163.

82. Magee, J.C., and Grienberger, C. (2020). Synaptic plasticity forms and functions. Annu. Rev. Neurosci. *43*, 95–117. https://doi.org/10.1146/annurev-neuro-090919-022842.

83. Krupa, D.J., Ghazanfar, A.A., and Nicolelis, M.A. (1999). Immediate thalamic sensory plasticity depends on corticothalamic feedback. Proc. Natl. Acad. Sci. USA *96*, 8200–8205. https://doi.org/10.1073/pnas.96.14.8200.

84. Butts, D.A., Kanold, P.O., and Shatz, C.J. (2007). A burst-based "hebbian" learning rule at retinogeniculate synapses links retinal waves to activity-dependent refinement. PLoS Biol. *5*, e61. https://doi.org/10.1371/journal.pbio.0050061.

85. Krahe, T.E., and Guido, W. (2011). Homeostatic plasticity in the visual thalamus by monocular deprivation. J. Neurosci. *31*, 6842–6849. https://doi.org/10.1523/JNEUROSCI.1173-11.2011.

86. Taylor, J.A., Hasegawa, M., Benoit, C.M., Freire, J.A., Theodore, M., Ganea, D.A., Innocenti, S.M., Lu, T., and Gründemann, J. (2021). Single cell plasticity and population coding stability in auditory thalamus upon associative learning. Nat. Commun. *12*, 2438. https://doi.org/10.1038/s41467-021-22421-8.

87. Ding, Y., Li, J., Clark, J., Diaz, F.G., and Rafols, J.A. (2003). Synaptic plasticity in thalamic nuclei enhanced by motor skill training in rat with transient middle cerebral artery occlusion. Neurol. Res. *25*, 189–194. https://doi.org/10.1179/016164103101201184.

88. Schuessler, F., Dubreuil, A., Mastrogiuseppe, F., Ostojic, S., and Barak, O. (2020). Dynamics of random recurrent networks with correlated low-rank structure. Phys. Rev. Res. *2*, 013111. https://doi.org/10.1103/PhysRevResearch.2.013111.

89. Huber, D., Gutnisky, D.A., Peron, S., O'Connor, D.H., Wiegert, J.S., Tian, L., Oertner, T.G., Looger, L.L., and Svoboda, K. (2012). Multiple dynamic representations in the motor cortex during sensorimotor learning. Nature *484*, 473–478. https://doi.org/10.1038/nature11039.

90. Peters, A.J., Chen, S.X., and Komiyama, T. (2014). Emergence of reproducible spatiotemporal activity during motor learning. Nature *510*, 263–267. https://doi.org/10.1038/nature13235.

91. Masamizu, Y., Tanaka, Y.R., Tanaka, Y.H., Hira, R., Ohkubo, F., Kitamura, K., Isomura, Y., Okada, T., and Matsuzaki, M. (2014). Two distinct layer-specific dynamics of cortical ensembles during learning of a motor task. Nat. Neurosci. *17*, 987–994. https://doi.org/10.1038/nn.3739.

92. Biane, J.S., Scanziani, M., Tuszynski, M.H., and Conner, J.M. (2015). Motor cortex maturation is associated with reductions in recurrent connectivity

among functional subpopulations and increases in intrinsic excitability. J. Neurosci. *35*, 4719–4728. https://doi.org/10.1523/JNEUROSCI.2792-14.2015.

93. Biane, J.S., Takashima, Y., Scanziani, M., Conner, J.M., and Tuszynski, M.H. (2019). Reorganization of recurrent layer 5 corticospinal networks following adult motor training. J. Neurosci. *39*, 4684–4693. https://doi.org/10.1523/JNEUROSCI.3442-17.2019.
94. Wang, M.B., and Halassa, M.M. (2022). Thalamocortical contribution to flexible learning in neural systems. Network Neuroscience *6*, 980–997. https://doi.org/10.1162/netna00235.
95. Hosp, J.A., Pekanovic, A., Rioult-Pedotti, M.S., and Luft, A.R. (2011). Dopaminergic projections from midbrain to primary motor cortex mediate motor skill learning. J. Neurosci. *31*, 2481–2487. https://doi.org/10.1523/JNEUROSCI.5411-10.2011.
96. Qian, L., Ko, H., Qian, Z.M., Yan, L.Y.C., Chan, D.C.W., Arbuthnott, G., Ke, Y., and Yung, W.H. (2017). Refinement of learned skilled movement representation in motor cortex deep output layer. Nat. Commun. *8*, 15834. https://doi.org/10.1038/ncomms15834.
97. Sampathkumar, V., Miller-Hansen, A., Sherman, S.M., and Kasthuri, N. (2021). Integration of signals from different cortical areas in higher order thalamic neurons. Proc. Natl. Acad. Sci. USA *118*, e2104137118. https://doi.org/10.1073/pnas.2104137118.
98. Phillips, J.W., Schulmann, A., Hara, E., Winnubst, J., Liu, C., Valakh, V., Wang, L., Shields, B.C., Korff, W., Chandrashekar, J., et al. (2019). A repeated molecular architecture across thalamic pathways. Nat. Neurosci. *22*, 1925–1935. https://doi.org/10.1038/s41593-019-0483-3.
99. Gu, Q.L., Lam, N.H., Wimmer, R.D., Halassa, M.M., and Murray, J.D. (2021). Computational circuit mechanisms underlying thalamic control of attention. Preprint at bioRxiv. https://doi.org/10.1101/2020.09.16.300749.
100. Mante, V., Sussillo, D., Shenoy, K.V., and Newsome, W.T. (2013). Context-dependent computation by recurrent dynamics in prefrontal cortex. Nature *503*, 78–84. https://doi.org/10.1038/nature12742.
101. Sussillo, D., Churchland, M.M., Kaufman, M.T., and Shenoy, K.V. (2015). A neural network that finds a naturalistic solution for the production of muscle activity. Nat. Neurosci. *18*, 1025–1033. https://doi.org/10.1038/nn.4042.
102. Barak, O. (2017). Recurrent neural networks as versatile tools of neuroscience research. Curr. Opin. Neurobiol. *46*, 1–6. https://doi.org/10.1016/j.conb.2017.06.003.
103. Lakshminarasimhan, K.J., Avila, E., Pitkow, X., and Angelaki, D.E. (2023). Dynamical latent state computation in the posterior parietal cortex. Nat. Commun. *14*, 1832. https://doi.org/10.1038/s41467-023-37400-4.
104. Guo, A.R.G., Guo, W.W., Zheng, J., Lee, A., Lez, J.R.-G., Li, N., Macklin, J.J., Phillips, J.W., Mensh, B.D., Branson, K., and Hantman, A.W. (2015). Cortex commands the performance of skilled movement. Elife *4*, e10774. https://doi.org/10.7554/eLife.10774.

STAR★METHODS

KEY RESOURCES TABLE

REAGENT or RESOURCE	SOURCE	IDENTIFIER
Software and algorithms		
tc-learning	This paper	github.com/kaushik-l/tc-learning
Deposited data		
ALM and thalamus data	Guo et al.[10]	DANDI: dandiarchive.org/dandiset/000009

RESOURCE AVAILABILITY

Lead contact

Further information and requests for resources should be directed to and will be fulfilled by the lead contact, Sean Escola (gse3@columbia.edu).

Materials availability

This study did not generate new unique reagents.

Data and code availability

- The study did not generate any new data. The DOI for the repository containing the data reanalyzed from previous work is listed in the key resources table.
- The code for simulating the models described in this study are available on github. The DOI is listed in the key resources table.
- Any additional information required to perform the simulations reported in this paper is available from the lead contact upon request.

METHOD DETAILS

Task description

We trained networks separately to solve three different types of tasks based on experiments that study computations underlying different functions – motor control, working memory, and goal-directed reaching. The motor control task tests the ability of networks to generate complex temporal patterns (like electromyograms) autonomously in the absence of external inputs. The working memory task tests how well networks maintain the identity of transient inputs, shortly after they have been removed. The reaching task tests a combination of the above two skills: the ability to remember a transiently cued target location, and then generate an appropriate movement pattern to reach that location upon the arrival of a go cue.

Motor control

The input $\mathbf{x}(t)$ is set to zero. The target function is a sum of sinusoidal functions, $y^*(t) = \sum_i w_i \sin\left(\frac{2\pi c t f_i}{T}\right)$, where $\mathbf{f} = [1, 2, 4, 6]$ denotes the frequencies of the sinusoids, $\mathbf{w} = [1, 0.75, 0.5, 0.25]$ denotes their relative strengths, and T is the total duration. In the basic version of the task, we set $c = 2$ and $T = 20\tau$ where τ is the time-constant of the cortical neurons. Task complexity is controlled by varying c from 1 to 5 which has the effect of scaling all frequency components of the target function by the same factor.

Working memory

The input $\mathbf{x}(t)$ is a pulse with one of P possible amplitudes A_p spaced evenly between $+1$ and -1 and a duration of 10τ. The goal is to reproduce the input amplitude during the subsequent delay period, so the target is a constant function $y^*(t) = A_p$ for a period of 30τ after the end of the input pulse. The basic version of the task corresponds to $P = 8$. Task complexity is controlled by varying P from 1 to 16 on a logarithmic scale.

Reaching

The input $\mathbf{x}(t) \in \mathbb{R}^2$ comprises the target location encoded in the amplitude of a 2D pulse of duration 4τ, and the go signal encoded in a step function $1_{t<g}$ where $g \in (5\tau, 20\tau)$ denotes the variable timing of the go signal. The goal is to generate a 2D output pattern that is zero for $t < g$, and subsequently deliver appropriate torques to control a two-link arm, such that the endpoint of the arm reaches the target location within a period of 10τ. The moment of inertia of the arms was taken to be unity such that the amount of torque applied is identical to the angular acceleration of the arms. The precise temporal pattern of angular acceleration, $\mathbf{y}^*(t)$ needed to perform successful reaching was obtained by training a recurrent neural network via backpropagation through time. The function $\mathbf{y}^*(t)$ was then used as the target function for training biologically plausible models.

Thalamocortical model

The thalamocortical model has a network architecture in which N interconnected cortical neurons is reciprocally connected with M uncoupled thalamic neurons where $\ll N$. In this model, the cortical population activity $\mathbf{h}$ depends on thalamic activity $\mathbf{r}$ and external input $\mathbf{x}$ according to Equation 1, $\tau\dot{\mathbf{h}}_t = -\mathbf{h}_t + \varphi(\boldsymbol{W}^{CC}\mathbf{h}_t + \boldsymbol{W}^{CT}\mathbf{r}_t + \boldsymbol{W}^{I}\mathbf{x}_t)$, where the nonlinearity $\varphi(\cdot)$ is the tanh function. The thalamic activity depends only on cortical activity as there is no recurrence within the thalamus, $\mathbf{r}_t = \varphi(\boldsymbol{W}^{TC}\mathbf{h}_t)$, and the network output is assumed to be a linear readout of the cortical activity: $\mathbf{y}_t = \boldsymbol{W}^{O}\mathbf{h}_t$. Simulations were performed using a timestep, dt = 10 ms, and the neuronal time constant was set to τ = 100 ms (10 timesteps). The dimensionality of the network input, S, and the network output, R, are task specific. S is 0,1, and 3 respectively for motor control, working memory, and reaching. R = 1 for motor control and working memory tasks and R = 2 for reaching. The number of cortical units, N, is fixed at 256 and the number of thalamic units, M, is varied systematically from 1 to 256 on a logarithmic scale. Elements of the input weight matrix $\boldsymbol{W}^{I}$ and the recurrent weight matrix $\boldsymbol{W}^{CC}$ are Gaussian, sampled from $\mathcal{N}(0, 1/S)$ and $\mathcal{N}(0, g^2/N)$, respectively. The strength of recurrent connectivity was chosen such that the network operated in the chaotic regime, g = 1.5. Output weights $\boldsymbol{W}^{O}$ are sampled from a uniform distribution, $\mathcal{U}(0, 2/N)$. Thalamocortical weights $\boldsymbol{W}^{CT}$ are sampled from $\mathcal{N}(0, g^2/M)$.

Connection sparsity in the cortex is controlled by varying the fraction of cortical neurons that each cortical neuron makes a synaptic contact with (f). The fraction is varied from $f = 1/N$ (very sparse) to f = 1 (fully connected) on a log scale. To ensure that the variance of total input current into single neurons remains independent of connection sparsity, we sampled the elements of $\boldsymbol{W}^{CC}$ from $\mathcal{N}(0, g^2/(fN))$. The dynamical regime of the cortex is controlled by varying the strength of recurrence within the cortex, $g = [0.5, 0.75, 1.0, 1.25, 1.5]$. For the simulations in which we vary the output dimensionality, we use variants of the motor control and working memory tasks with $R = [1, 2, 3, 4]$ outputs. In all simulations, we used a timestep dt = 0.1*τ where τ is the neuronal time constant. A table of simulation parameters that were varied in individual analyses is included in Table S1.

Learning algorithm

Thalamocortical weights are trained using a biologically plausible algorithm called Random Feedback Local Online, RFLO [39] (Figures 2, 3, 4, and 5). With the exception of Figure 1 (see below), we use meta-learning to optimize corticothalamic weights while learning thalamocortical weights concurrently via RFLO [40,41](Figure 2).

RFLO

The goal of learning is to minimize the discrepancy between the network output and a desired target function. Therefore, the loss function is taken to be the squared-error across all output units, integrated over time where the error in dimension r of the output is the difference between the target and the actual output of the network in that dimension, $\varepsilon_r(t) = y_r^*(t) - y_r(t)$.

$$L = \frac{1}{2T}\sum_{t=1}^{T}\sum_{r=1}^{R}[\varepsilon_r(t)]^2 \qquad \text{(Equation 3)}$$

The weight updates in RFLO are derived by making three approximations to standard gradient-based algorithms that minimize the loss with respect to the weights. The first approximation consists of dropping nonlocal terms from the gradient, so that computing the update to a given synaptic weight requires only pre- and postsynaptic activities, rather than information about the entire state of the cortex including all of its synaptic weights. Second, we project the error back into the cortical network for learning using random feedback weights $\boldsymbol{B}$ sampled from $\mathcal{U}(0, 2/N)$, rather than feedback weights that are precisely tuned to match the readout weights. This relaxation is made possible by learning readout weights in conjunction with thalamocortical weights. Third, the weight updates are performed in real-time instead of accumulating gradients and updating the weights at the end of each trial. The resulting update rules for thalamocortical weights $\boldsymbol{W}^{CT}$ and readout weights $\boldsymbol{W}^{O}$ are given by:

$$\delta\boldsymbol{W}_{ij}^{O} = \eta\varepsilon_i(t)h_j(t) \qquad \text{(Equation 4)}$$

where h_j is the activity of cortical unit i, $\boldsymbol{W}_{ij}^{O}$ denotes the readout weight from cortical unit j to output unit i, and η is the learning rate. This is sometimes also referred to as the delta rule.

$$\delta\boldsymbol{W}_{ij}^{CT} = \eta[\boldsymbol{B}\boldsymbol{\varepsilon}(t)]_i p_{ij}(t) \qquad \text{(Equation 5)}$$

where $\boldsymbol{W}_{ij}^{CT}$ denotes the thalamocortical weight from thalamic unit j onto cortical unit i; p_{ij} denotes the eligibility trace that accumulates the correlation between the activity of the (presynaptic) thalamic unit j and the (postsynaptic) cortical unit i: $\tau\dot{p}_{ij} = -p_{ij}(t) + \varphi'(u_i(t))r_j(t)$ where r_j is the activity of thalamic unit j, $u_i = \sum_j \boldsymbol{W}_{ij}^{CC}h_j + \sum_j \boldsymbol{W}_{ij}^{CT}r_j + \sum_j \boldsymbol{W}_{ij}^{I}x_j$ is the total input current to cortical unit i, and α is the leak rate of the cortical units. For the simulation in Figure 1C, the update rule for the update rule for corticocortical weights $\boldsymbol{W}^{TC}$ is given by:

$$\delta\boldsymbol{W}_{ij}^{TC} = \eta[\boldsymbol{B}'\boldsymbol{\varepsilon}(t)]_i q_{ij}(t) \qquad \text{(Equation 6)}$$

where $\boldsymbol{W}_{ij}^{TC}$ denotes the corticothalamic weight from cortical unit j onto thalamic unit i; q_{ij} denotes the eligibility trace defined as the product of the activity of the (presynaptic) cortical unit j and the (postsynaptic) thalamic unit i: $q_{ij} = \varphi'(v_i(t))h_j(t)$ where h_j is the activity of cortical unit j, $v_i = \sum_j \boldsymbol{W}_{ij}^{TC} h_j$ is the total input current to thalamic unit i. $\boldsymbol{B}'$ denotes the random feedback weights through which error signals arrive at the thalamus. Elements of $\boldsymbol{B}'$ are sampled from $\mathcal{U}(0, 2/M)$. Prior to learning, thalamocortical weights and readout weights are both initialized randomly by sampling from $\mathcal{N}(0, g^2/M)$ and $U(0, 2/N)$ respectively. The learning rate was set to $\eta = 0.1$ for readout and thalamocortical weight updates, and the training was performed for $K = 10,000$ trials unless specified otherwise. The learning rate for corticothalamic weights for the simulation in Figures 1C and 1D was determined by hyperparameter optimization.

Meta-learning

We use meta-learning to determine the optimal structure of corticothalamic projection that supports biologically plausible of thalamocortical weights. Corticothalamic weights W^{TC} are initialized randomly at the beginning of the meta-learning procedure by sampling from $\mathcal{N}(0, 1/N)$, and weights are updated using backpropagation through time at the end of each epoch containing $K = 200$ learning trials. The objective is to minimize the average loss $\bar{L}$ across trials of the epoch, $\bar{L} = \frac{1}{K}\sum_k L_k$ where the loss in each trial L_k is given by Equation 3. Thalamocortical weights W^{CT} are reinitialized randomly at the beginning of each epoch by sampling from $\mathcal{N}(0, g^2/M)$, and weights are updated using RFLO according to Equation 5. We considered a model with $N = 256$ cortical neurons and $M = 32$ thalamic neurons. Meta-learning was used to update corticothalamic weights onto only one of the thalamic units. Optimization is performed for 10,000 epochs using Adam optimizer with a learning rate of 0.0001. By restricting meta-learning to a single thalamic unit, we can readily evaluate the relative optimality of the different strategies used in Figure 2 by measuring the alignment of the meta-optimized corticothalamic weights with the readout direction and the principal component direction. To ensure that this technique promotes learning specifically via thalamocortical synapses, we fixed all other weights and enforced feedback alignment ($\boldsymbol{B}^T = \boldsymbol{W}^O$). For simulations in Figure S2A, we relax this constraint and update both readout and corticothalamic weights.

Subspace aligned models of corticothalamic connectivity

We consider three types of thalamocortical models that differ in the structure of corticothalamic connectivity for the simulations shown in Figure 3.

Random

In this version of the model, elements of $\boldsymbol{W}^{TC}$ are sampled randomly from $\mathcal{N}(0, 1/N)$. Therefore, the thalamic activity in this model corresponds to a random low-dimensional projection of the cortical activity. These weights are held fixed throughout learning.

Principal component

In this strategy, elements of $\boldsymbol{W}^{TC}$ are proportional to the M leading eigenvectors U of the covariance in cortical population activity, where the constant of proportionality is $1/\sqrt{N}$. The resulting thalamic activity corresponds to the M leading principal components of the cortical activity. Since the structure of cortical dynamics changes during thalamocortical learning, corticothalamic weights are dynamically updated in this version at the end of each learning trial: $\boldsymbol{W}_{k+1}^{TC} = (1 - \beta)\boldsymbol{W}_k^{TC} + \beta U_k$ where U_k denotes the leading eigenvectors of the cortical covariance at the end of k trials, and $\beta = 0.01$ is the corticothalamic learning rate. The dynamic updating of corticothalamic weights in this manner corresponds to a Hebbian learning strategy operating at the corticothalamic synapses. We also trained a variant of this strategy where individual principal components are distributed across all M thalamic neurons instead of being segregated in individual neurons. This variant was constructed by multiplying the corticothalamic weights that yield segregated PCs, by a random orthonormal matrix.

Readout

This version of the model is characterized by a perfect alignment between readout weights $\boldsymbol{W}^O$ and corticothalamic weights onto a small subset of the thalamic units. This subset contains a maximum of R units whose activity mirrors the network output, where R denotes the number of output units. Corticothalamic projections onto the remaining $M - R$ thalamic units are sampled randomly from $\mathcal{N}(0, 1/N)$. Similar to the principal component strategy, the corticothalamic weights onto the subset of R thalamic neurons are updated dynamically: $\boldsymbol{W}_{k+1}^{TC} = (1 - \beta)\boldsymbol{W}_k^{TC} + \beta \boldsymbol{W}_k^O$ where $\boldsymbol{W}_k^O$ denotes the readout weights at the end of k trials and $\beta = 1$. This strategy is analogous to a pathway that carries signals from cortex to thalamus via axon collaterals. For models with $M > R$, we also trained a variant of this strategy where the R-dimensional readout signal is distributed across all M thalamic neurons instead of being concentrated in R neurons. This variant was constructed by multiplying the corticothalamic weights by a random orthonormal matrix.

Models of distributed thalamic representation with partial subspace alignment of corticothalamic connectivity

For the simulations shown in Figure 4, we constructed networks that differed in the number of cortical neurons ranging from $N = 64$ to $N = 2048$. For each of these networks, we simulated models of thalamocortical learning with large and moderate compression ratios ($M/N = 100$ and $M/N = 10$) where M was rounded up to the nearest integer. Depending on the task, we used structured corticothalamic projections partially aligned with either the readout direction (for motor control) or the leading principal component (for working memory) by varying the parameter ρ as explained below. Note that all other simulations of subspace-aligned models correspond to setting $\rho = 1$ for corticothalamic weights onto one thalamic neuron.

Principal component

In this strategy, elements of $\boldsymbol{W}^{\mathrm{TC}}$ are configured such that each thalamic neuron receives a weighted sum of the leading principal component (PC) of the cortical population activity and a random direction from the $N-1$ dimensional subspace orthogonal to the leading principal component. The i^{th} row is given by $\boldsymbol{W}_i^{\mathrm{TC}} = \frac{\rho}{\sqrt{M}}\mathbf{u} + \sqrt{1-\rho^2}\mathbf{u}_{\perp,i}$ where $\mathbf{u}$ is the leading eigenvector of the covariance matrix of the cortical population activity and $\mathbf{u}_{\perp,i}$ denotes a random linear combination of the remaining eigenvectors. ρ controls the fraction of variance in the leading PC explained by the thalamic neuron. Because the random component is on average uncorrelated across neurons, the fraction of total variance in the leading PC collectively explained by the thalamic population is ρ^2.

Readout

In this strategy, elements of $\boldsymbol{W}^{\mathrm{TC}}$ are configured such that each thalamic neuron receives a weighted sum of the signal in the readout direction of the cortical population activity and a random direction from the $N-1$ dimensional subspace orthogonal to the leading principal component. The i^{th} row is given by $\boldsymbol{W}_i^{\mathrm{TC}} = \frac{\rho}{\sqrt{M}}\mathbf{W}^{\mathrm{O}} + \sqrt{1-\rho^2}\mathbf{W}^{\mathrm{O}}_{\perp,i}$ where $\mathbf{u}$ is the leading eigenvector of the covariance matrix of the cortical population activity and $\mathbf{W}^{\mathrm{O}}_{\perp,i}$ denotes a random linear combination of the remaining eigenvectors. The fraction of total variance in the readout collectively explained by the thalamic population is ρ^2.

QUANTIFICATION AND STATISTICAL ANALYSIS

Each model tested in this study was simulated 40 times with different parameter initializations, and those initializations were identical across models sharing similar architecture. Unless specified otherwise, we used median as the summary statistic and error bars denote standard errors estimated by bootstrapping.

Task performance

We quantify task performance as $1-R^2 = \frac{\sum_k \mathrm{Var}[y_k^* - y_k]}{\sum_k \mathrm{Var}[y_k^*]}$ and $\mathrm{Var}[\cdot]$ denotes variance across time. For tasks with multiple conditions – Working memory and Reaching – the outputs from different conditions were concatenated before computing R^2. A value of 0 corresponds to perfect performance, while 1 corresponds to chance level. Note that this measure reduces to the loss L defined in Equation 3 when the target function has unit temporal variance.

Alignment between weights

We quantified the alignment between pairs of weight vectors $\mathbf{m}$ and $\mathbf{n}$ by taking their normalized dot product $\frac{(\mathbf{m}\cdot\mathbf{n})}{\|\mathbf{m}\|\|\mathbf{n}\|}$ where $\|\cdot\|$ denotes the ℓ_2 norm. For computing feedback alignment in the cortex (Figure 1C), $\mathbf{m} = \boldsymbol{B}$ and $\mathbf{n} = \boldsymbol{W}^{\mathrm{O}}$ where $\boldsymbol{B}$ denotes the feedback weights projecting the error signal to cortical neurons. For computing feedback alignment in the thalamus (Figure 1C), $\mathbf{m} = \boldsymbol{B}'$ and $\mathbf{n} = \boldsymbol{W}^{\mathrm{CT}}\varphi'(\mathbf{u}_t)\boldsymbol{W}^{\mathrm{O}}$ where $\boldsymbol{B}'$ denotes the feedback weights projecting the error signal to thalamic neurons. The alignment between optimized corticothalamic weights and readout weights is computed by taking, $\mathbf{m} = \boldsymbol{W}^{\mathrm{TC}}$ and $\mathbf{n} = \boldsymbol{W}^{\mathrm{O}}$. The alignment between optimized corticothalamic weights and principal component weights is computed by taking, $\mathbf{m} = \boldsymbol{W}^{\mathrm{TC}}$ and $\mathbf{n} = \boldsymbol{z}$, where $\boldsymbol{z}$ denotes the leading eigenvector of the cortical covariance matrix.

Neural datasets

Detailed experimental methods for behavioral and neural recordings in the motor control task and working memory task are described in[14,104] and[10] respectively. In the motor control task,[14] neural recordings were performed simultaneously in the motor cortex and motor thalamus while mice performed a reach-to-grasp movement to grab a food pellet (Figure 6A – left). The dataset includes one behavioral session each from 3 different mice. The mean number of cortical and thalamic units was 53 ± 9 and 33 ± 5 respectively. In the working memory task,[10] recordings were performed in separate sessions in the frontal cortex, specifically anterior lateral motor cortex (ALM), and thalamus, specifically ventral medial (VM) and ventral anterior–lateral (VAL) nuclei, while mice performed a delayed discrimination task to detect (by whisking) and report (by licking left/right) the location of a pole (anterior/posterior) following a delay of ~ 1.3 s after the pole was removed (Figure 6B – left). The dataset includes 5 behavioral sessions from one mouse. The total number of cortical and thalamic units was 151 and 72 respectively.

Estimation of readout weights

We estimated the readout weights for both tasks by regressing behavior against the activity of the population of cortical neurons. We split the trials into a training set (80% for estimating weights), a validation set (10% for hyperparameter optimization), and a test set (10% for computing variance explained R^2).

For the motor control task, behavior was defined as the time-varying acceleration profile of the hand. To obtain acceleration profiles, hand position traces were first aligned to the onset of hand movement and averaged across trials in the training set. We then numerically computed the second derivative to obtain the average acceleration profile along the three axes $(a_x(t), a_y(t), a_z(t))$. Likewise, we aligned spike trains of motor cortex neurons to the onset of hand movement, convolved them with a Gaussian function (width σ as hyperparameter), and computed the trial-averaged population activity, $\mathbf{h}(t)$ in the training set. We regressed the

acceleration profiles against the population activity to estimate the readout weights $\widehat{\mathbf{w}}_x^{\mathrm{O}}$, $\widehat{\mathbf{w}}_y^{\mathrm{O}}$, and $\widehat{\mathbf{w}}_z^{\mathrm{O}}$ using ordinary least squares, and optimized the smoothing parameter σ by cross-validation. Finally, we expressed the readout weights in the basis of the principal components (PC) of the population activity. To do this, we first performed eigendecomposition of the population covariance, $\langle \mathbf{h}\mathbf{h}^{\mathrm{T}} \rangle = U\Lambda U^{\mathrm{T}}$, and then projected the estimated readout weights for each component of acceleration onto the top $k = 16$ eigenvectors, e.g., $\widehat{\mathbf{w}}_{\mathrm{PC},x}^{\mathrm{O}} = \widehat{\mathbf{w}}_x^{\mathrm{O}} U_{1:k}$. Since the weight profiles of the three components of acceleration were qualitatively similar in the PC basis, we averaged them to obtain a single readout weight profile for the motor control task ($\widehat{\mathbf{w}}_{\mathrm{PC}}^{\mathrm{O}} = \frac{1}{3}(|\widehat{\mathbf{w}}_{\mathrm{PC},x}^{\mathrm{O}}| + |\widehat{\mathbf{w}}_{\mathrm{PC},y}^{\mathrm{O}}| + |\widehat{\mathbf{w}}_{\mathrm{PC},z}^{\mathrm{O}}|)$).

For the working memory task, behavior was defined as the choice made on each trial. We aligned spike trains of ALM neurons to the onset of the delay period, convolved them with a Gaussian function (width σ as hyperparameter), and averaged them separately across trials with leftward and rightward choices ($\mathbf{h}_l(t)$ and $\mathbf{h}_r(t)$). We restricted out analysis to trials in which the choice was correct. We concatenated the response from the two sets of trials ($\mathbf{h}(t) = [\mathbf{h}_l(t)\ \mathbf{h}_r(t)]$) and used them as predictors in a linear regression model to decode choice, $c(t) = [c_l(t)\ c_r(t)]$, where $c_l(t) = -1$ and $c_r(t) = +1$. As in the motor control task, readout weights $\widehat{\mathbf{w}}^{\mathrm{O}}$ were estimated using ordinary least squares, and we optimized the smoothing parameter σ by cross-validation. Finally, we expressed the readout weights in the basis of the principal components (PC) of the population activity to obtain $\widehat{\mathbf{w}}_{\mathrm{PC}}^{\mathrm{O}}$.

Analysis of corticothalamic communication

For estimating corticothalamic weights, we used a procedure similar to the one outlined above, except now the activity of cortical neurons $\mathbf{h}(t)$ was used to decode the activity of individual thalamic neurons $r(t)$, instead of decoding behavior. We used the principal components of cortical activity as predictors instead of raw firing rates. Specifically, we first performed eigendecomposition of the population covariance, $\langle \mathbf{h}\mathbf{h}^{\mathrm{T}} \rangle = U\Lambda U^{\mathrm{T}}$, and projected the cortical activity onto the top k eigenvectors, $\mathbf{h}_k(t) = \mathbf{h}(t)U_{1:k}$. We then estimated the regression weights to decode $r(t)$ from $\mathbf{h}_k(t)$. By varying k from 1 to 16, we estimated the corticothalamic weights $\widehat{\mathbf{w}}_k^{\mathrm{TC}}$ that captured the influence of the top k principal components of cortical activity on each thalamic neuron. The cumulative variance in the thalamic neuron activity explained by the top k cortical principal components was quantified using the coefficient of determination, $R^2(k) = 1 - \frac{\mathrm{Var}[r(t) - \widehat{\mathbf{w}}_k^{\mathrm{TC}}\mathbf{h}(t)]}{\mathrm{Var}[r(t)]}$. Finally, we divided the cumulative variance explained by k principal components by the variance explained all $K = 16$ principal components to obtain a normalized measure of variance explained, $R^2(k)/R^2(K)$, for each thalamic neuron in the dataset.

Cell Reports, Volume *43*

Supplemental information

Specific connectivity optimizes learning in thalamocortical loops

Kaushik J. Lakshminarasimhan, Marjorie Xie, Jeremy D. Cohen, Britton A. Sauerbrei, Adam W. Hantman, Ashok Litwin-Kumar, and Sean Escola

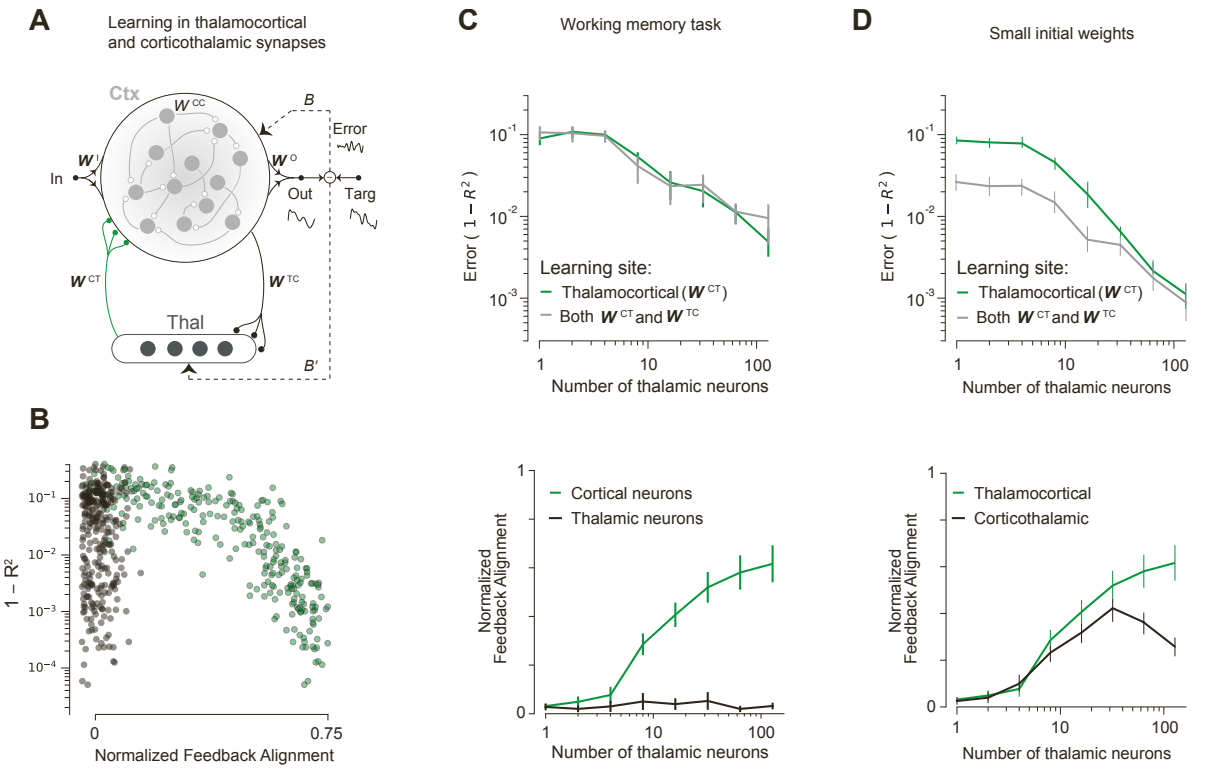

Figure S1: **Local plasticity of thalamocortical and corticothalamic synapses**. Related to Figure 1. **A.** Corticocortical weights ($\boldsymbol{W}^{\mathrm{CC}}$) are fixed. A local learning rule (RFLO, see text) is applied to simultaneously update thalamocortical weights ($\boldsymbol{W}^{\mathrm{CT}}$) and corticothalamic weights ($\boldsymbol{W}^{\mathrm{TC}}$). Error signals are projected to the cortex (via $\boldsymbol{B}$) and thalamus (via $\boldsymbol{B}'$) to facilitate learning in thalamocortical and corticothalamic synapses respectively. **B.** Across simulations, feedback alignment in the cortex predicts learning performance (green circles), but feedback alignment in the thalamus is uncorrelated with learning performance (black circles). **C**. Top: Learning performance of a model in which plasticity was restricted to thalamocortical synapses (green), compared with the performance of a model in which there was plasticity at both sites (gray) in the working memory task. Bottom: The alignment between feedback weights ($\boldsymbol{B}$) and readout weights ($\boldsymbol{W}^{\mathrm{O}}$) in cortical neurons (**A**). Alignment between feedback weights ($\boldsymbol{B}'$) and effective readout weights ($\boldsymbol{W}^{\mathrm{CT}}\phi'(\mathbf{u}_t)\boldsymbol{W}^{\mathrm{O}}$, see Methods) in thalamic neurons (**B**). $\mathbf{u}_t = \boldsymbol{W}^{\mathrm{CT}}\mathbf{r}_t$ denotes the membrane potential of cortical neurons. **D.** Learning performance (top) and feedback alignment (bottom) when initial corticothalamic weights are drawn from a distribution with variance $\sim O(1/N)$ (see text). All models have N = 256 cortical neurons.

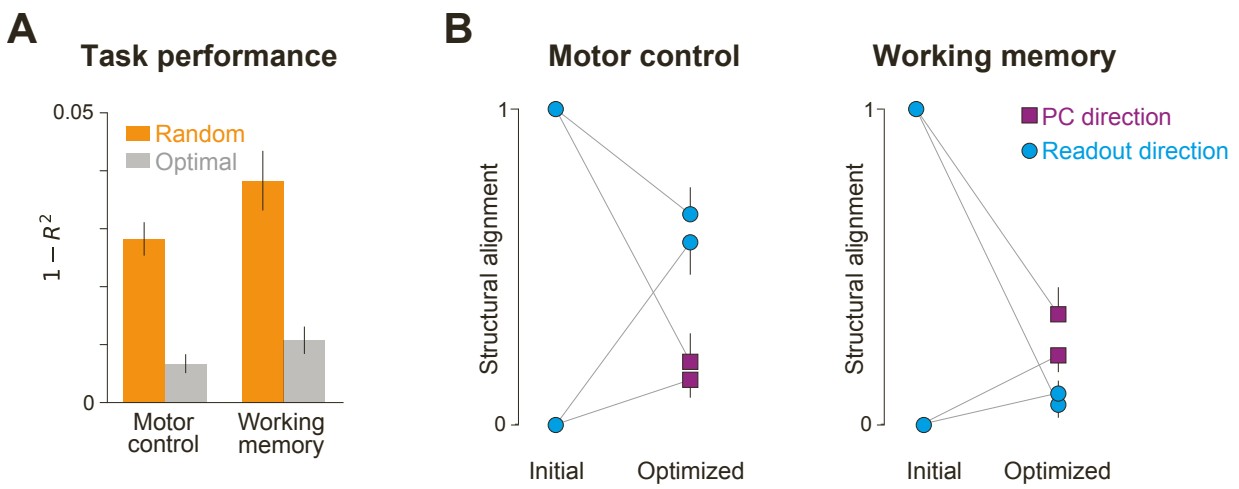

Figure S2: **Robustness of optimized corticothalamic weights determined by meta-learning**. Related to Figure 2. **A.** Models with optimized corticothalamic connectivity outperform models with random connectivity even when both thalamocortical and readout weights are updated in parallel. In these models, the component of optimized corticothalamic weights aligned with readout weights is updated during the learning phase, while keeping the orthogonal components fixed. **B.** The degree of alignment of optimized corticothalamic weights with readout and principal component directions does not depend on the alignment of the model at the beginning of meta-learning. In these models, corticothalamic weights are either orthogonal or perfectly aligned with the readout direction in the beginning of the meta-learning phase ("Initial") but the final alignments are qualitatively similar ("Optimized"). Error bars denote standard errors estimated by bootstrapping. All models have N = 256 cortical neurons and M = 32 thalamic neurons.

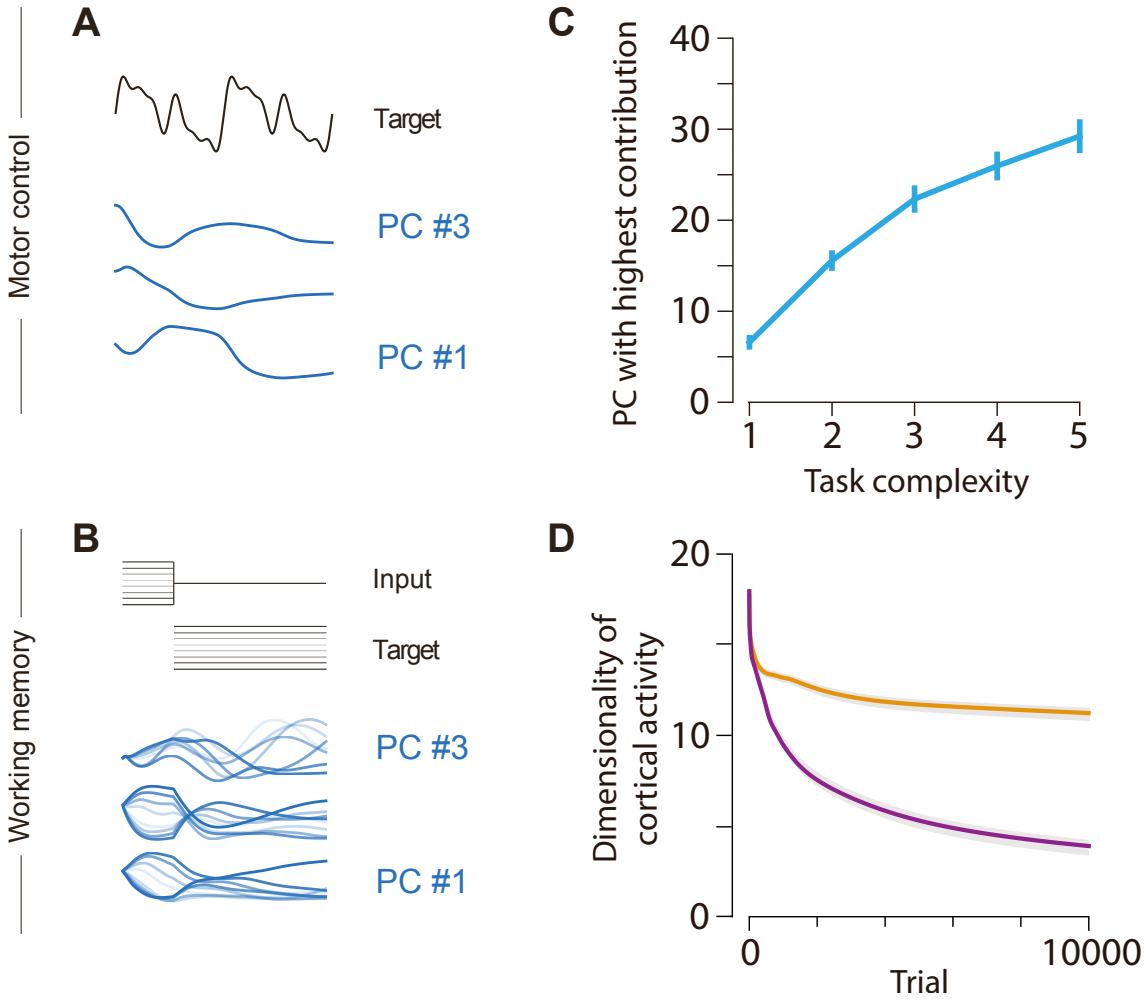

Figure S3: **Model principal components**. Related to Figure 3. **A-B.** The target function (black), and the top three principal components of cortical activity (blue traces) at the beginning of learning. Individual traces in **B** correspond to response to inputs with different amplitudes. All models have N = 256 cortical neurons and M = 16 thalamic neurons. **C.** The principal component with the highest contribution to readout weights as a function of the complexity of the motor control task (see Methods for how complexity is varied). **D.** Evolution of the dimensionality of the cortical activity across learning in models with random (orange) or PC-aligned (purple) corticothalamic weights trained on the working memory task. Dimensionality was estimated by computing the participation ratio of the covariance in cortical activity. Error bars denote ±1SEM estimated by bootstrapping.

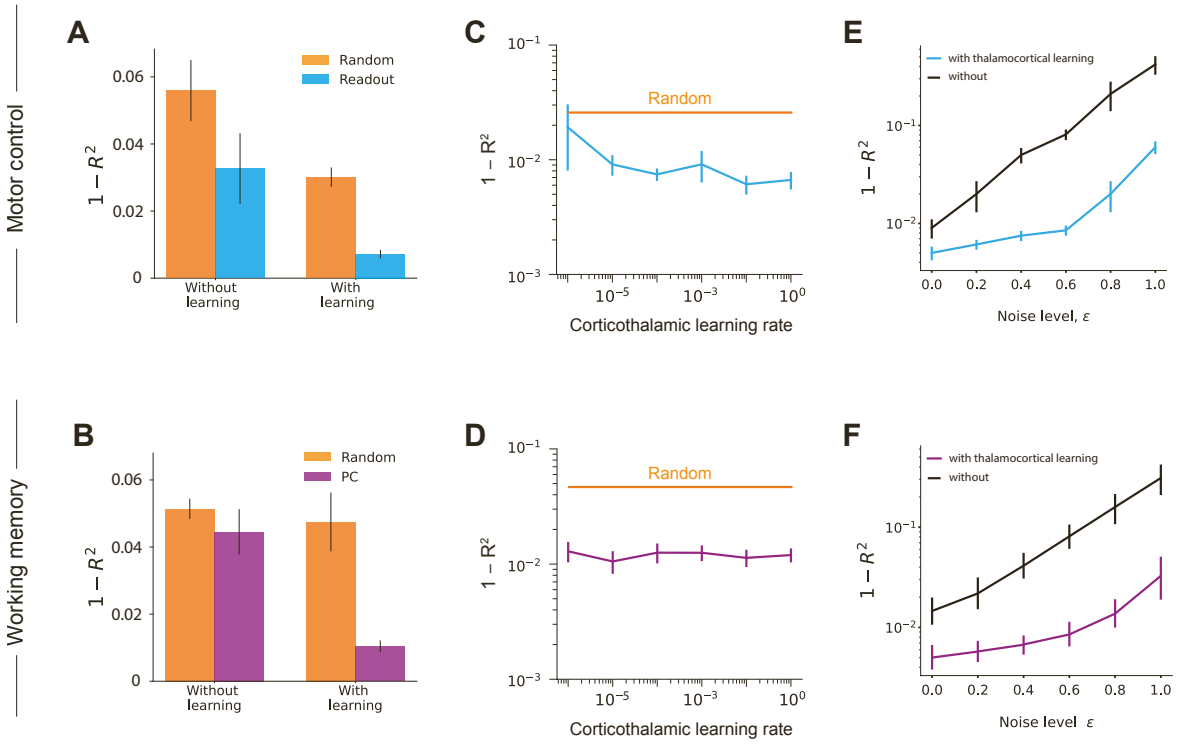

Figure S4: **Significance and robustness of subspace aligned corticothalamic connectivity models**. Related to Figure 3. **A-B.** Task performance of models with and without learning in thalamocortical synapses. In the motor control task (**A**), models differed in terms of whether corticothalamic weights are random or aligned with readout, whereas in the working memory task (**B**), models differed in terms of whether corticothalamic weights are random or aligned with the principal component. Readout weights are updated in all models. **C-D.** Learning performance of models in which corticothalamic weights were slowly updated to align with readout or principal component: $\mathbf{W}_k^{\mathrm{TC}} = (1-\beta) * \mathbf{W}_{k-1}^{\mathrm{TC}} + \beta * u$, where u denotes either readout (**C**) or principal component (**D**), and β denotes the speed of update. **E-F.** Performance of models as a function of noise in the initial condition, drawn from a uniform distribution $U[-\epsilon, +\epsilon]$. In both sets of tasks, the model with thalamocortical learning (cyan and purple) is more robust to noise than the model in which only readout weights are learned (black).

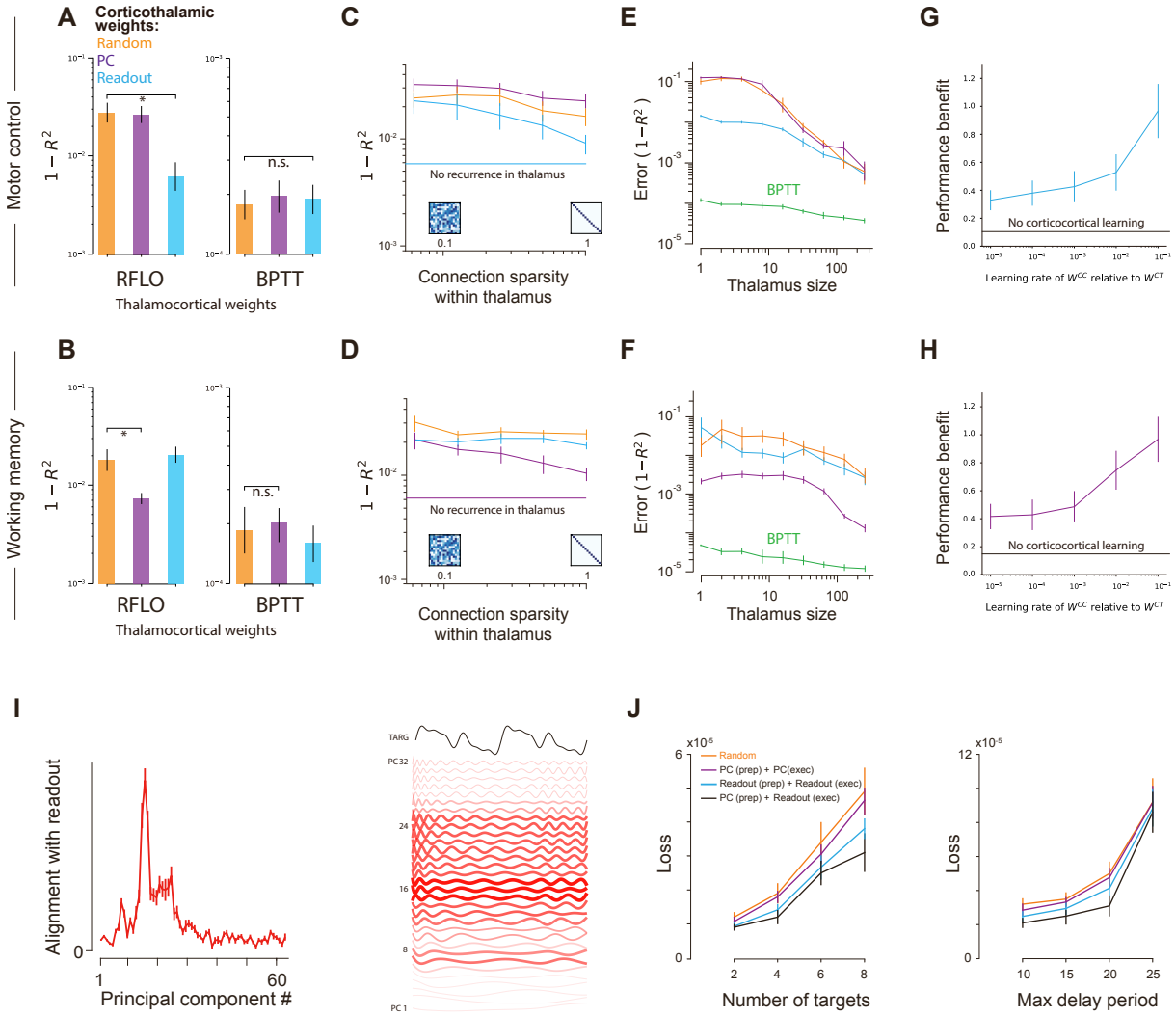
A
Corticothalamic weights:
Random
PC
Readout
Motor control
1 − R²
*
n.s.
RFLO
BPTT
Thalamocortical weights
C
No recurrence in thalamus
Connection sparsity within thalamus
E
Error (1 − R²)
BPTT
Thalamus size
G
Performance benefit
No corticocortical learning
Learning rate of W^CC relative to W^CT
B
Working memory
D
F
H
I
Alignment with readout
Principal component #
TARG
PC 32
PC 1
J
x10⁻⁵
Random
PC (prep) + PC(exec)
Readout (prep) + Readout (exec)
PC (prep) + Readout (exec)
Loss
Number of targets
Max delay period

Figure S5: **Alternative forms of learning**. Related to Figures 4&5. **A-B.** Effect of corticothalamic structure on thalamocortical weights are updated using RFLO and BPTT for motor control and working memory tasks. **C-D.** Effect of adding recurrence within thalamus on thalamocortical learning. f_{thal} denotes the fraction of thalamic neurons that do not receive recurrent inputs from other thalamic neurons. Black solid line denotes performance of the model without thalamic recurrence. **E-F.** Learning performance of a model where corticothalamic weights are updated using BPTT (green) relative to fixed corticothalamic weights of different structures. **G-H.** Performance benefit of models when corticocortical weights are updated (using RFLO) in conjunction with thalamocortical weights. Errors are normalized by those of a null model with random corticothalamic weights. Values less than 1 indicate a benefit for structured corticothalamic weights (the lower the better). **I. Principal components**. Left: The relative contribution of different principal components to the readout weights in the motor control task. Right: Top 32 principal components of the cortical activity. Thickness and saturation of the components are adjusted based on their contribution to the readout. The target function is shown in black. **J. Goal-directed reaching**. Left: The models in which corticothalamic weights onto thalamic neurons active during preparation (execution) are aligned with the cortical principal component (readout) learn better than models with other structures, regardless of the number of reach targets. Right: Similar to left panel, but showing learning performance as a function of the maximum delay between the location stimulus and the go cue. Note that in each condition, the delay was stochastic and drawn from a uniform distribution, $\mathcal{U}[5, t_{\max}]$, where $t_{\max}$ denotes the maximum delay period in units of neuronal time constant τ.

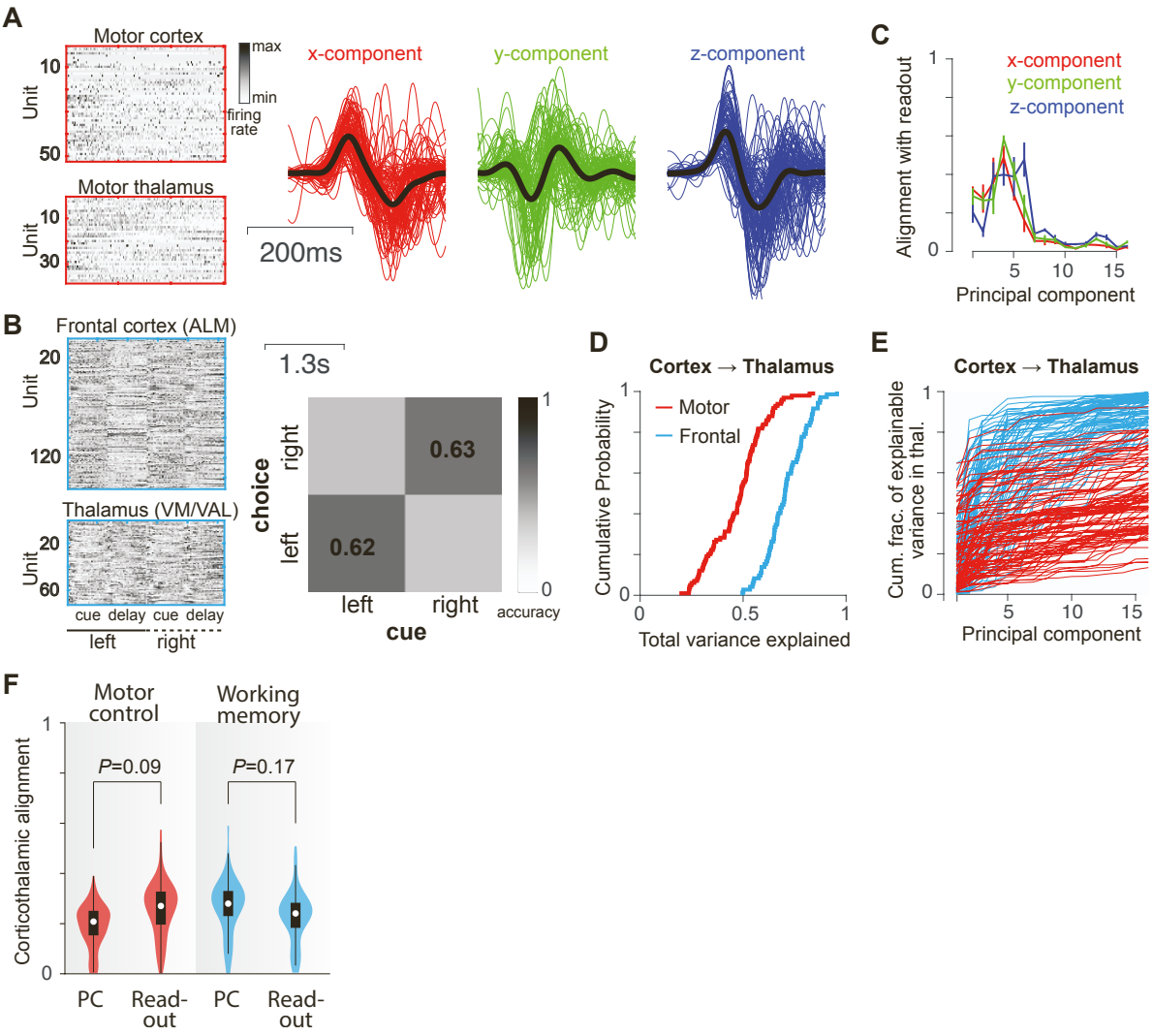
A
Motor cortex
Unit
10
50
max
min
firing rate
Motor thalamus
Unit
10
30
x-component
y-component
z-component
200ms
C
Alignment with readout
1
0
x-component
y-component
z-component
5
10
15
Principal component
B
Frontal cortex (ALM)
Unit
20
120
Thalamus (VM/VAL)
Unit
20
60
cue delay cue delay
left
right
1.3s
choice
right
left
0.63
0.62
left
right
cue
1
0
accuracy
D
Cortex → Thalamus
Cumulative Probability
1
0
Motor
Frontal
0
0.5
1
Total variance explained
E
Cortex → Thalamus
Cum. frac. of explainable variance in thal.
1
0
5
10
15
Principal component
F
Motor control
Working memory
Corticothalamic alignment
1
0
P=0.09
P=0.17
PC
Read-out
PC
Read-out

Figure S6: **Corticothalamic interactions in mice performing motor control and working memory tasks**. Related to Figure 6. **A.** Left: Data from[14]. Trial-averaged response matrix of neurons in the motor cortex (top) and motor thalamus (bottom) during the pellet grasping task, between onset and end of movement. Rows denote units and columns denote time. Response of each neurons is z-scored for the purpose of visualization. Right: Three spatial components of hand acceleration. Traces from individual trials are shown in color, and black traces denote the average across trials. **B.** Left: Data from[10]. Similar to **A** (left), but during the delayed discrimination task. Response from trials with leftward and rightward responses were separately averaged and concatenated. Each trial comprised a ∼1.3s cue period followed by a ∼1.3s delay period. Right: Confusion matrix showing the choice accuracy in the leftward and rightward conditions. **C.** Mean alignment (across sessions) between the direction of readout weights and different cortical PCs, in the motor control task. Alignment of readout weights corresponding to each of the three spatial components of acceleration are shown separately (only the acceleration component with the highest variance (z-component) was shown in Figure 6). Error bars denote ±1 SEM. **D.** Cumulative probability distribution of the variance explained in the activity of thalamic neurons when decoding all neurons recorded from the cortex. Note that in all analysis, the ALM cortical population (n=151) was subsampled to match the dataset from motor cortex (n=53 ± 9). **E.** The fraction of explainable variance in individual thalamic neurons, as a function of the number of cortical principal components. Each curve denotes one thalamic neuron recorded during the motor control (red) and working memory (blue) tasks. **F.** Alignment of corticothalamic weights of individual thalamic neurons in the two datasets with the direction of the leading principal component of cortical activity and the readout direction. White dots denote the median, black boxes denote inter-quartile range and black lines denote adjacent values. Statistics of a one-sided paired t-test are shown.

Table S1. **Simulation settings**. Weights in the network were structured, random, or learned. The learning rate was set using hyperparameter optimization everywhere unless noted otherwise.

Figure panel	Corticocortical weights, W^{CC}	Thalamocortical weights, W^{CT}	Corticothalamic weights, W^{TC}	Readout weights, W^{O}	Feedback weights, B
1C – green curve	Fixed, random	Updated using RFLO	Fixed, random	Updated using delta rule	Random
1C – gray curve	Fixed, random	Updated using RFLO	Updated using RFLO	Updated using delta rule	Random B Random B'
S1C	Fixed, random	Updated using RFLO	Updated using RFLO	Updated using delta rule	Random B Random B'
S1D	Fixed, random	Updated using RFLO starting from a small value	Updated using RFLO	Updated using delta rule	Random B Random B'
2D, E	Fixed, random	Updated using RFLO	Updated using BPTT in outer-loop	Fixed	Aligned with readout
S2A	Fixed, random	Updated using RFLO	Updated using BPTT in outer-loop	Updated using delta rule	Random
S2B	Fixed, random	Updated using RFLO	Updated using BPTT in outer-loop	Fixed	Aligned with readout
3	Fixed, random	Updated using RFLO	Fixed, random or structured as indicated	Updated using delta rule	Random
S3C	Fixed, random	Updated using RFLO	Structured ; Partially aligned with readout	Updated using delta rule	Random
S3D	Fixed, random	Updated using RFLO	Structured	Updated using delta rule	Random
S4	Fixed, random	Fixed or Updated using RFLO, as indicated	Fixed, random or structured as indicated	Updated using delta rule	Random
4A,C	Fixed, random	Updated using RFLO	Partially aligned with readout	Updated using delta rule	Random
4B,D	Fixed, random	Updated using RFLO	Partially aligned with leading PC	Updated using delta rule	Random
5	Fixed, random	Updated using RFLO	Structured; Two readout-aligned weights and two PC-aligned weights	Updated using delta rule	Random
S5A,B	Fixed, random	Updated using RFLO or BPTT, as indicated	Fixed, random or structured as indicated	Updated using delta rule	Random
S5C,D	Fixed, random	Updated using RFLO	Fixed, random or structured as indicated	Updated using delta rule	Random
S5E,F	Fixed, random	Updated using RFLO	Fixed, random, structured, or updated using BPTT as indicated	Updated using delta rule	Random
S5G,H	Updated using RFLO	Updated using RFLO	Structured	Updated using delta rule	Random
S6	Fixed, random	Updated using RFLO	Fixed, random or structured as indicated	Updated using delta rule	Random